

Chapter 15: Maps of Exogenic Structures

THE SURFACE of the Earth is shaped by a wide range of exogenic processes. Exogenic structures originate from processes at or near the surface of the Earth. In contrast, endogenic deformation structures are created by mechanisms originating from within the Earth. The structures discussed in preceding chapters are all formed by endogenic processes (e.g., folds, faults, igneous intrusions and extrusions). Four main types of exogenic structures are considered here: impact structures, landslides, sinkholes, and glacial structures. Knowledge of these distinct features is essential for interpreting geological maps correctly.

Contents: Impact structures are illustrated in section 15-1. Examples of landslides are discussed in section 15-2. Sinkholes and glacial patterns constitute sections 15-3 and 15-4, respectively.

15-1 Impact structures

The solar system formed about five billion years ago by gravitational accretion of matter from a solar nebula. The protoplanets formed in molten state, because the reduction of potential energy by the gravitational collapse of the solar matter released heat. The surfaces of the terrestrial planets had sufficiently cooled to solidify about four billion years ago. The surfaces of the Moon, and of Mars and Mercury are only minimally affected by erosion processes and display a large number of pristine *impact structures* or *astroblemes*, that have battered their crusts since their

early formation. Counting and dating of the lunar and Martian craters have revealed that the planets of the solar system suffered particularly frequent impacts about four billion years ago, when the majority of the craters were formed.

Size-frequency distribution counts further suggest that the Earth, also, must have hosted an enormous number of impact structures. Estimates for the past two billion years include twenty craters larger than one hundred kilometers in diameter, 6,000 craters of five to one hundred kilometers in diameter, and 100,000 craters of one to five kilometers in diameter. However, the

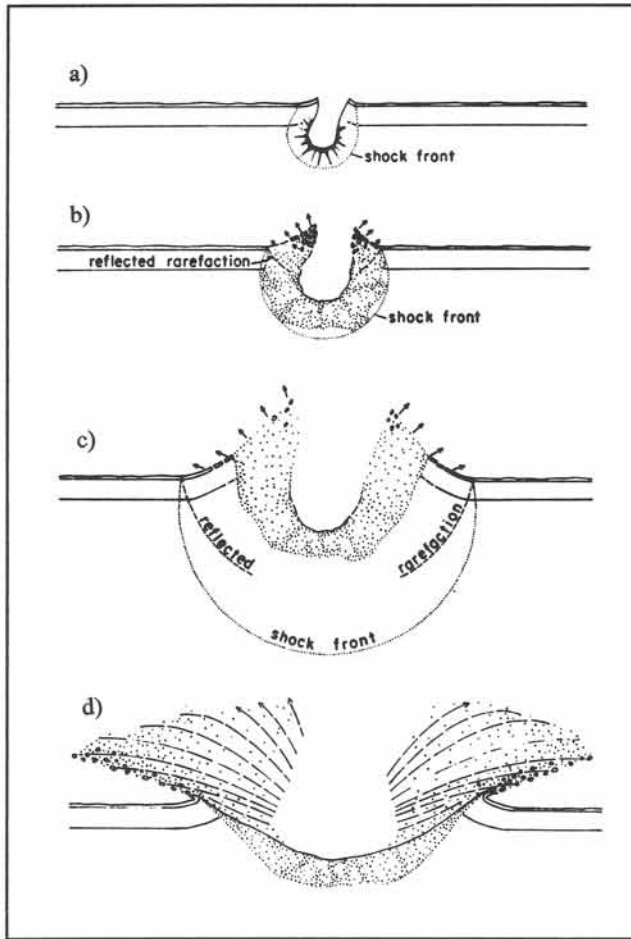
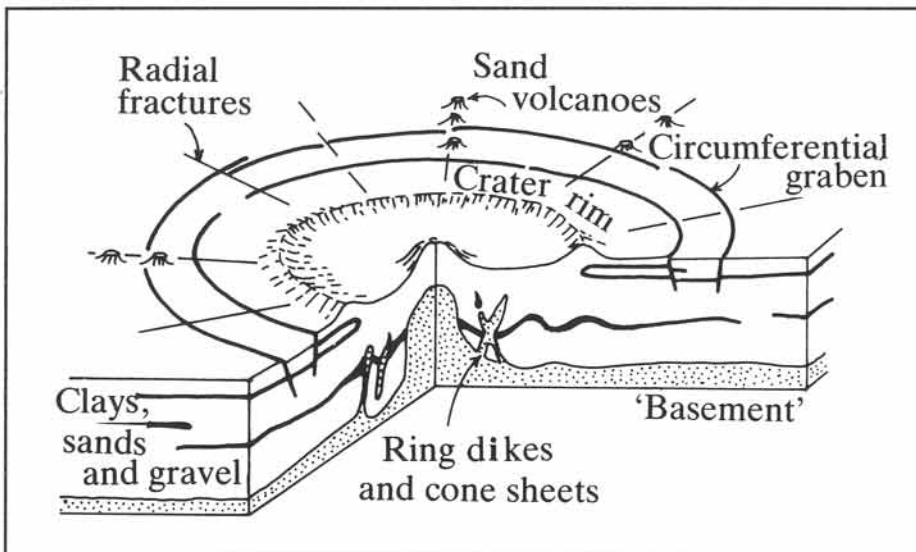


Figure 15-1: a) to d) Schematic cross-sections of a developing impact crater. a) Propagating shock front and expanding impact cavity. b) Shock front envelopes partly fused and brecciated rock. c) Material behind rarefaction limit, including meteoritic fragments, is ejected. d) Margins of the crater are backfolded, leaving debris inside and outside the crater wall.

average continental erosion rate of about one hundred meters per million years rapidly excavates and removes most of these impact structures. Consequently, we can expect to find only the remnants of relatively young impact structures or the scars of older impacts so big that they extended well below the reach of subsequent erosion depths. So far, only about two hundred impact craters have been convincingly identified on Earth; most of them are located in tectonically stable Precambrian terrains.

The formation of an *impact crater* is illustrated in Figure 15-1a to d. Rock, compressed by the initial impact, partly fractures and melts, but it, also, rebounds elastically to eject debris fragments and to backfold any sedimentary layers in the crater rim. The final crater morphology comprises an elevated rim, radial ejecta and fracture patterns, and a central depression -



sometimes hosting a central mound and circumferential or annular graben (Fig. 15-2a & b). The central mound occurs only in craters larger than about five kilometers and results from the tendency for the center to take up most of the elastic recovery, leaving an annular depression between the central mound and the crater rim (Fig. 15-2).

Systematic studies of impact structures received

Figure 15-2: Structural elements of an impact crater.

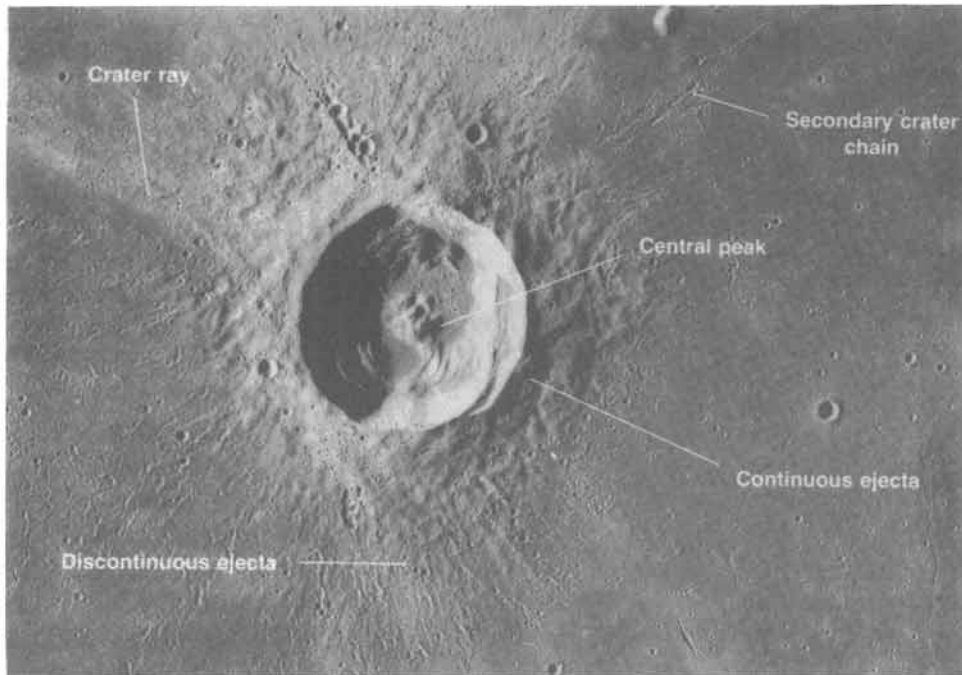


Figure 15-3a: Crater Euler and central peaks measure twenty kilometers across, Mare Imbrium, Moon.



Figure 15-3b: Crater Aristarchus, measuring forty kilometers across, with internal slump terraces, Moon.

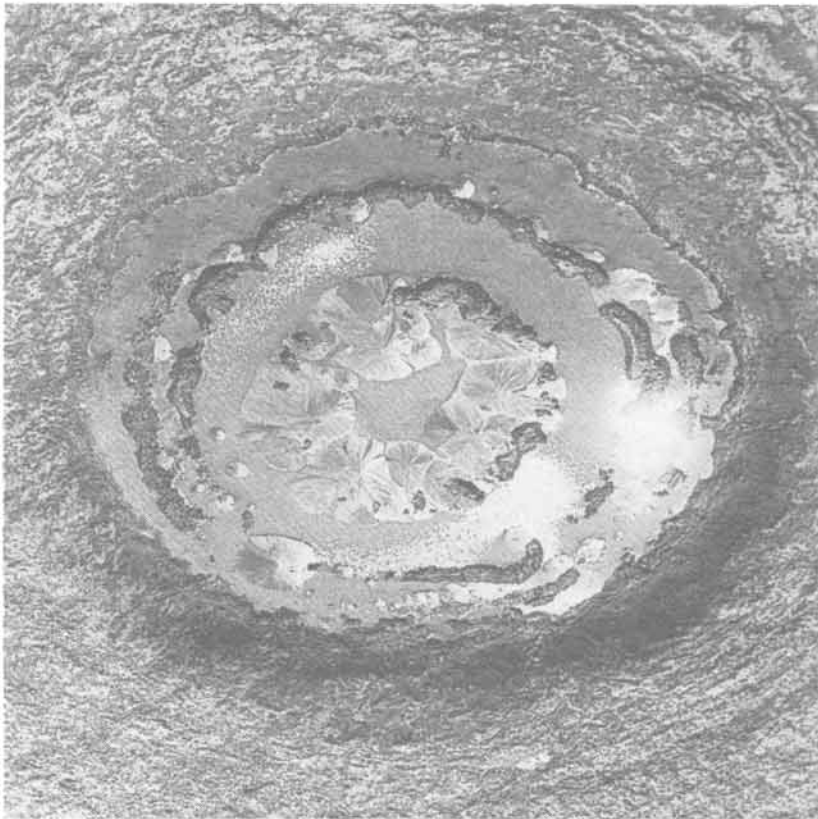


Figure 15-4: Crater caused by ground blast test. Internal slump terraces are partially submerged by ground water.

a major boost after detailed images of lunar craters were acquired by Apollo flights of the late 1960's and early 1970's (Figs. 15-3a & b). These

images provided clear examples of large impact craters with central mounds and internal slump terraces. Such slump terraces have been reproduced in experimental ground blasts, using dynamite to simulate the effect of a meteoritic impact (Fig. 15-4). The elevated crater rim is a rather characteristic feature of impact craters.

Theoretical studies show that only larger *meteorites*, with masses in excess of ten tons, have enough kinetic energy to break through the Earth's atmosphere without being slowed down. Their impact speeds are about ten to fifty kilometers per second. Bodies smaller than one ton completely disintegrate upon entry into the atmosphere. Parts of bodies of intermediate size may reach the Earth's surface, but with their speed greatly reduced, approaching free-fall velocities of about one hundred

meters per second. The well-known Meteor Crater, Arizona, 1.3 kilometers wide and two hundred meters deep (Fig. 15-5), is thought to

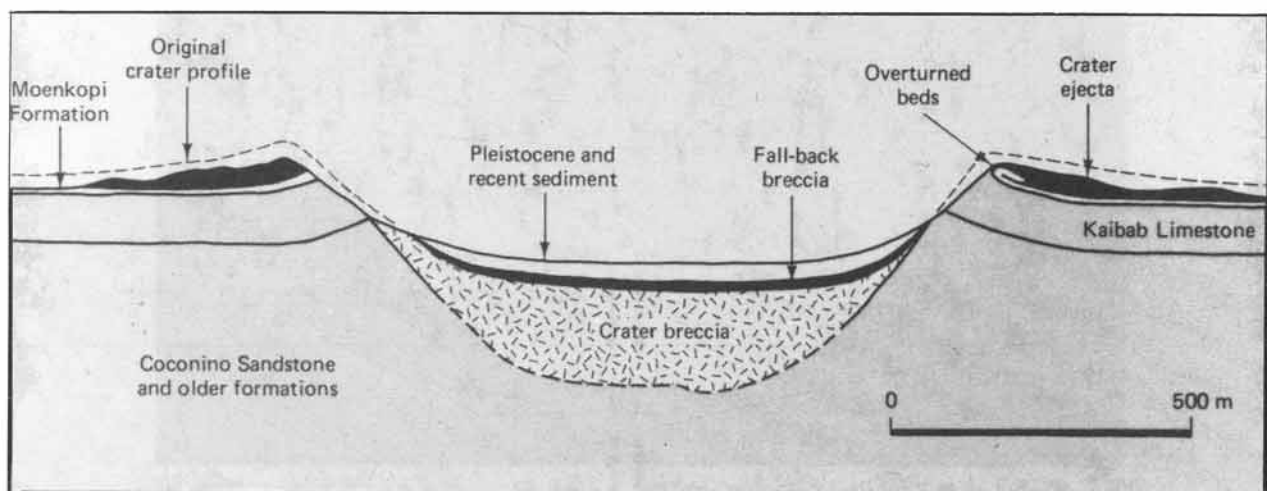


Figure 15-5: Geologic cross-section of Meteor Crater, Arizona.

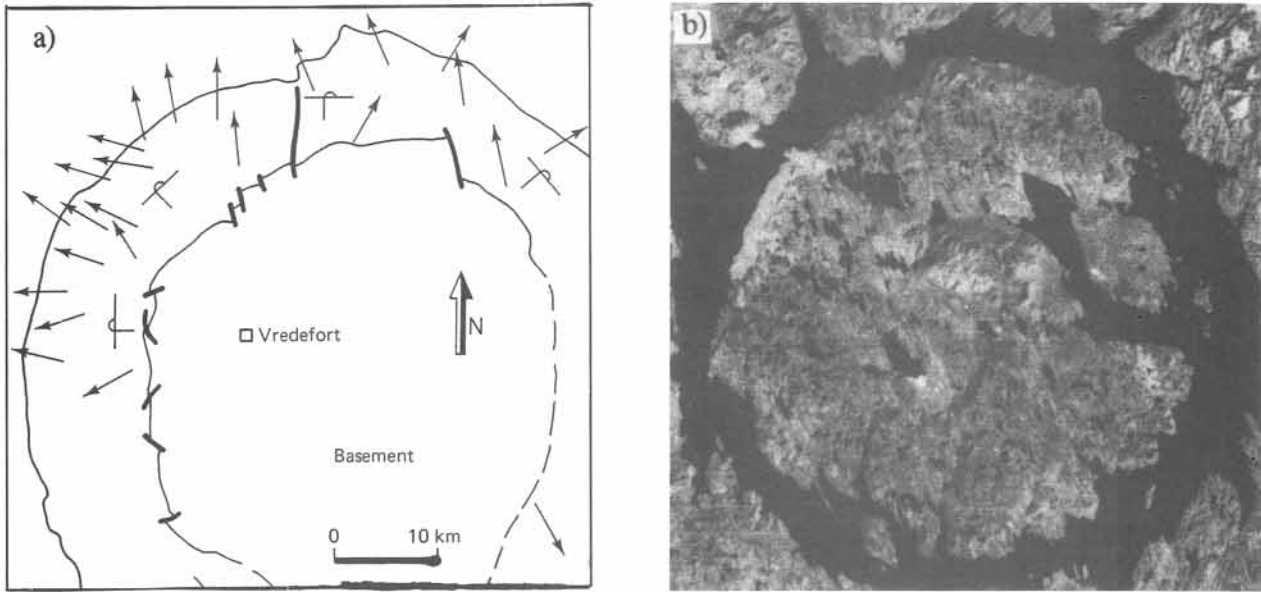
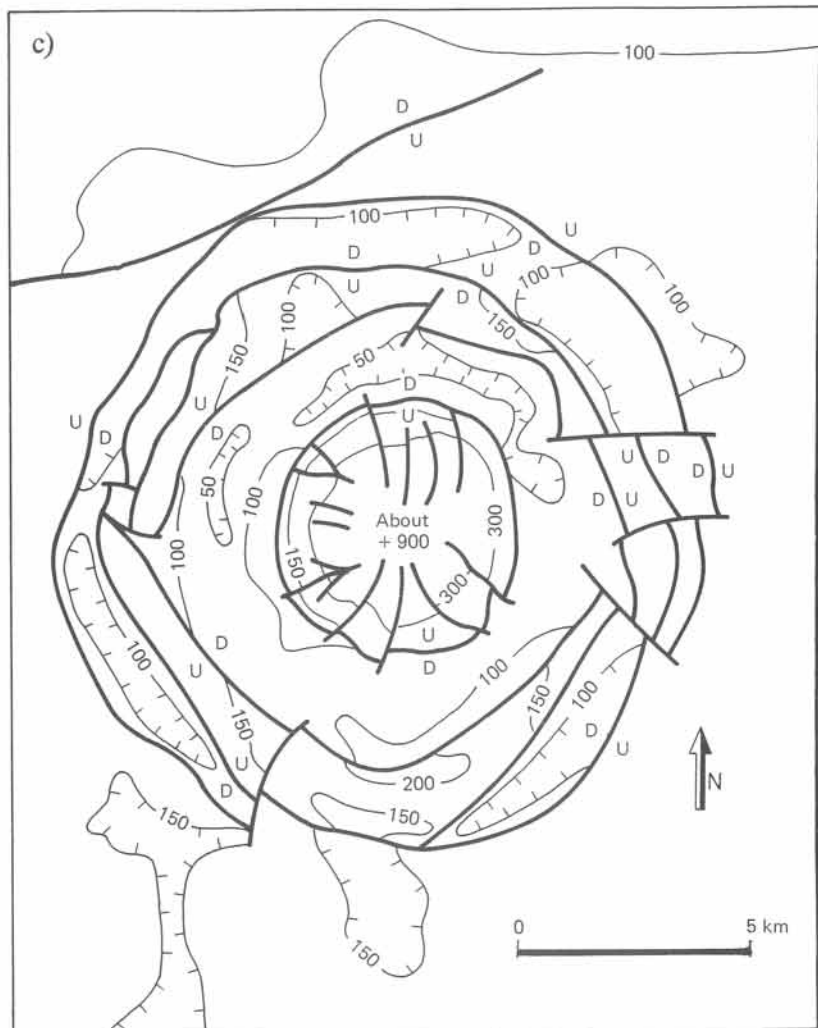


Figure 15-6: Sketch maps and Landsat image of impact structures (astroblemes): (a) Vredefort, South Africa, (b) Manicouagan, Quebec, and (c) Wells Creek, Tennessee. Arrows in the overturned rimrock at Vredefort indicate shockwave propagation direction, inferred from shatter cones.

have been formed by a meteorite of only 25 meters in diameter with an impact velocity of fifteen kilometers per second.

Many subcircular structures, now known to be of impact origin, were initially thought to be of igneous origin, because of the morphological similarities between impact craters and igneous craters. Additionally, impact melts may form rocks, resembling *pseudotachylites* and *rhyolites*. However, the backfolding of the crater rim, formation of certain high-pressure minerals,



impact breccias, and so-called *shatter cones* all are unique for impact craters. Some of the best investigated impact structures are: Meteor Crater, Arizona (1.2 km); Grosses Bluff, Australia (3 km); Wells Creek, Tennessee (10 km); Ries basin, Germany (20 km); Vredefort ring, South Africa (40 km); Siljan ring, Sweden (50 km), and the Manicouagan and Sudbury rings, Canada (66 and 100 km). A satellite image of the Manicouagan

astrobleme, impressed on the Canadian shield of Quebec, visualizes the broad central uplift and a water-filled peripheral depression (Fig. 15-6b). The Vredefort ring and Wells Creek structure are illustrated in the maps of Figure 15-6a and c.

The Siljan ring structure, Precambrian shield of Sweden, is a meteoritic impact crater with an outer rim diameter of 50 kilometers (Fig. 15-7a).

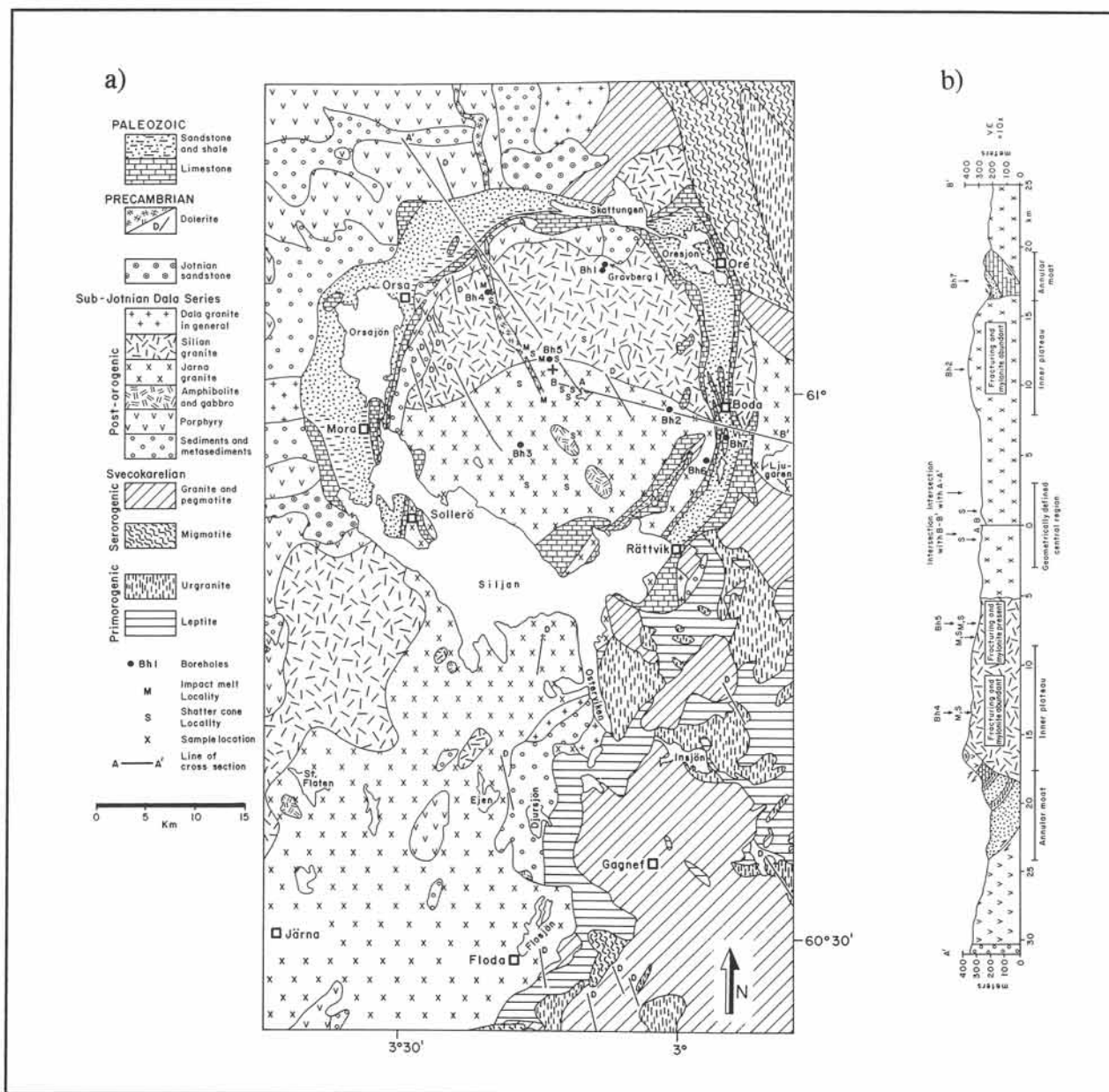


Figure 15-7: a) & b) Geological map and cross-section of the Siljan impact ring, central Sweden. Indicated are the locations of seven shallow boreholes (Bh1-Bh7) and the first of two deep wells (Gravberg 1).

Lower Paleozoic sedimentary rocks occupy an annular depression in the crater rim (Fig. 15-7b). The impact is of late Devonian age; it occurred about 360 million years ago. Two holes, up to seven kilometers deep, have been drilled into the floor of the Siljan crater. These expensive drillings explored for methane gas, that was speculated to have leaked from the mantle into fracture zones beneath the crater. Although huge quantities of methane are thought to occur dispersed in all planetary interiors, any fractures in the lower crust will heal and close by ductile creep. If any, significant gas concentrations in the Siljan area remain sealed in the mantle and were not encountered in any of the wells drilled.

□ **Exercise 15-1: Research possible impact feature(s) relatively near to your home region, and summarize the main features and estimated age.**

15-2 Landslides

Steeper slopes occupied by rock masses and soil may become unstable and collapse. The slope failure may involve movement of large volumes of rock, sometimes with devastating consequences if occurring in urban areas. A geological assessment, therefore, is important in the planning of new construction in order to investigate the stability of any slopes, supporting or surrounding the projected building site. An initial exami-

nation of existing survey maps may reveal whether any *landsliding* or *mass wasting* has been recognized in the area. The detached rock masses leave behind a distinct scar in the terrain with a typical spoon-shaped curvature (Fig. 15-8). The movement involves the formation of transverse normal faults across the slide mass with progressive loss of coherence, as the jumbled blocks move downward. The lower portion of the slump mass may consist of a *debris-flow*.

One of the grimmest examples of the seriousness of the threat posed by landsliding is illustrated by the 1970 rock avalanche of Yungay, Peru. A strong off-shore earthquake and the associated ground motion triggered the collapse of an already unstable north flank of the 6,700-meter-high Nevados Huascarán in the Peruvian Andes. A rock mass of millions of tons slid down the mountain side and fell for over one kilometer, disintegrating upon impact. It was accompanied by the melting of ice entrapped in the mass movement. The resulting debris-flow roared down the nearby valley floor, jumped a 200-meter-high ridge in the valley, and completely

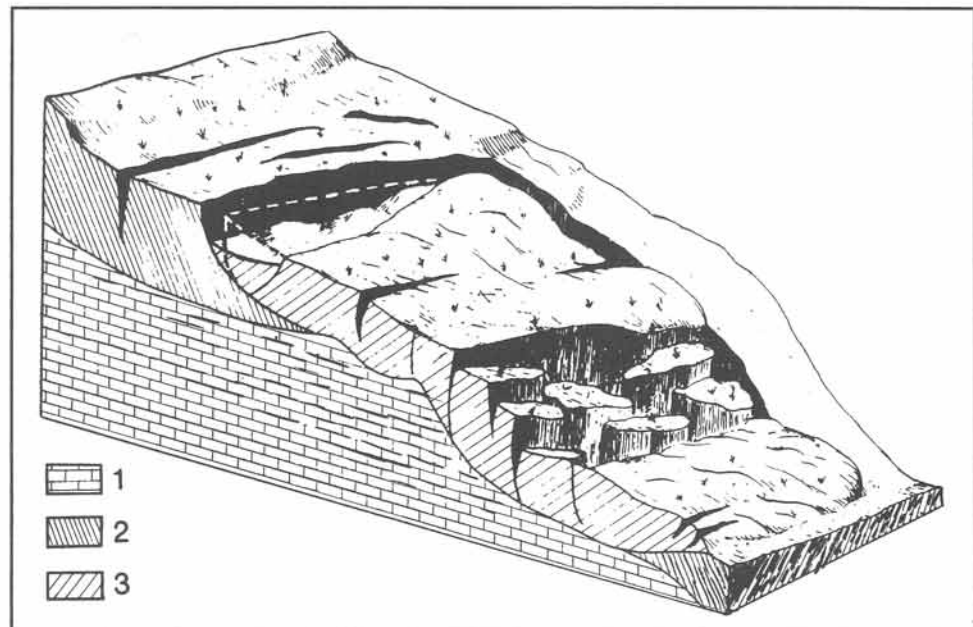


Figure 15-8: Block diagram of idealized landslide. Legend shows: (1) solid bed rock, (2) poorly consolidated soil, (3) slump mass.



Figure 15-9: a) & b) Views of the valley floor near Yungay: (a) before, and (b) after the arrival of a debris-flow from the Nevados Huascarán.

buried the adjacent town of Yungay, fourteen kilometers away from the Huascarán (Fig. 15-9a & b). Ranrahirca, another town close to Yungay, was, also, erased by the mass movement, causing a total death toll of 20,000 people. The whole tragedy was completed in a few minutes. Rock avalanches may reach speeds of 200 kilometers per hour. Part of the rock movement is facilitated by compressed air, trapped underneath the slide mass.

Figure 15-10 illustrates a four-kilometer-long debris-flow, covering the snout of the Sherman Glacier, Alaska, that was triggered by the 1964 earthquake of magnitude 8.5. The same earthquake set up a tsunami, which swept the coast of the Gulf of Alaska. An entire ocean front district of Anchorage, Turnagain Heights, collapsed by landsliding over a clay bed, liquefied by the water pressure (Fig. 15-11). The event caused 131 deaths. Sliding was extensive, also, at the town of Valdez, where 31 persons were killed when an entire dock slid into the ocean. In an unprecedented move, Valdez was abandoned and rebuilt on more stable ground, seven kilometers away from its 1964 location. Landsliding need not necessarily be triggered by seismic ground movement. Figure 15-12 illustrates the erosion of the coastline by landsliding at



Figure 15-10: A huge rock avalanche (dark) covers the snout of the Sherman Glacier, Alaska. It was triggered by the 1964 earthquake.

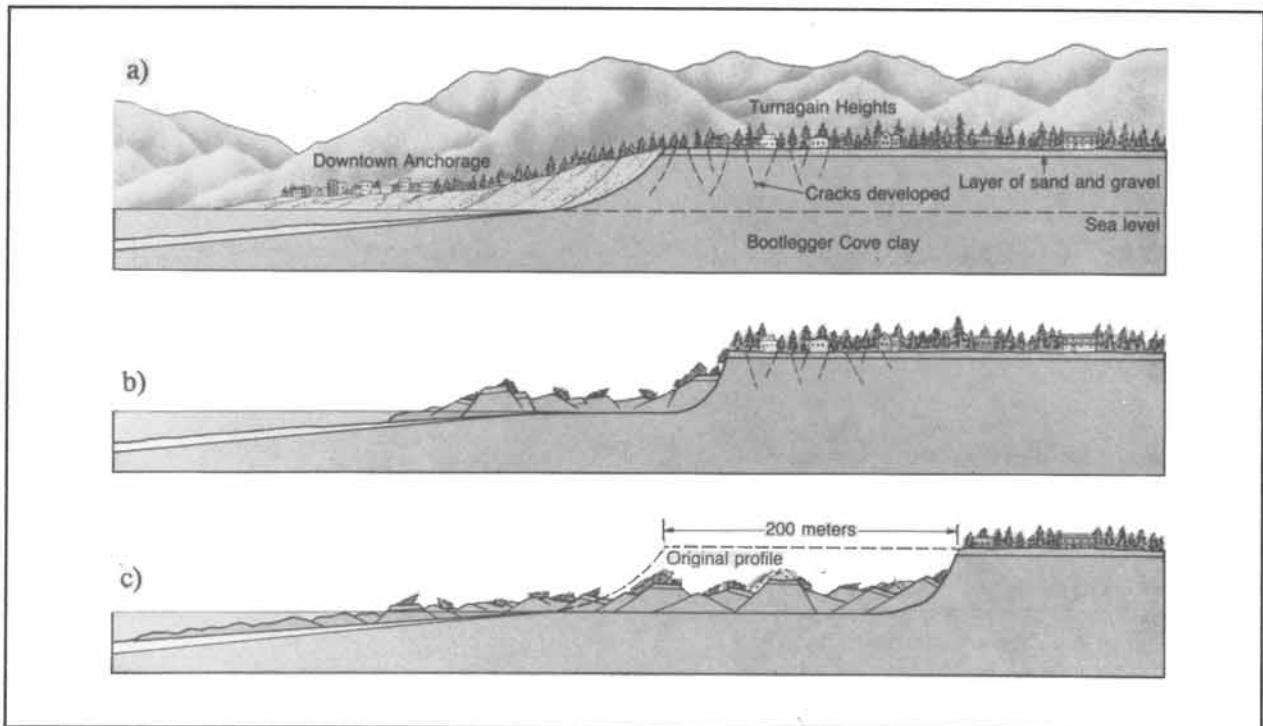


Figure 15-11: Collapse of the Turnagain Heights-district in Anchorage, Alaska, triggered by the 1964 earthquake. a) Opening of cracks, b) sliding, and c) final damage, five minutes after the onset of sliding.

Point Fermin, California. The major cause of sliding here is oversteepening of the cliffs. Obviously, the recurrence of multiple earthquakes in the region further contributes to the destabilization of the cliffs at Point Fermin.

Slides may, also, be triggered by an increase of the pore water pressure of rock formations, soaked by heavy rainfall or by the inadvertent effects of human construction work. The Vaiont Dam disaster, 1963, is a tragic example of construction with poor site investigation. The Vaiont Valley, Italy, was dammed by a 265-meter-tall hydropower dam, completed in 1960. The water reservoir, forming behind the dam, soaked the rocks of the walls of the Vaiont gorge. Creep of the walls, which included swelling clays and cavernous limestones, occurred at rates of one centimeter per week and speeded up to twenty centimeters per day in the weeks before the final collapse. Finally, Mount Toc's flank let loose 0.24 cubic kilometer of rock and debris, which filled the Vaiont Valley to 150 meters above the reservoir level (Fig. 15-13a). Consequently, the reservoir flooded the dam with a ninety-meter-

high wall of water, leaving the Vaiont Dam miraculously intact, but destroying everything else in its path downstream; about 2,600 deaths were counted. The landslides of both the Vaiont disaster and the Gros Ventre slide (see, also, Fig. 1-7b) resulted from the swelling of a layer of clay beneath a surface slope, which was subparallel to the stratigraphic dip, termed a dip-slope. Figure 15-13b is a north-south cross-section of the Vaiont Valley and outlines the failure surface of the slide mass. The failure started by swelling and detachment of the clay-bearing Malm formation. The section of the Gros Ventre slide, Wyoming, suggests a similar mechanism of failure (Fig. 15-14). The slide occurred after a period of extensive rainfall, which destabilized the sandstone bed on a dip-slope of water-saturated clays.

Landslides seldom occur without precedents. Areas frequently affected by landslides commonly are littered with deposits of *allochthonous* rock sheets and jostled debris. Figure 15-15 illustrates the morphology of an old landslide in the landscape. Figure 15-16a shows a detailed geological map of the oversteepened northern slope of the



Figure 15-12: Collapse of urbanized cliffs at Point Fermin, California.

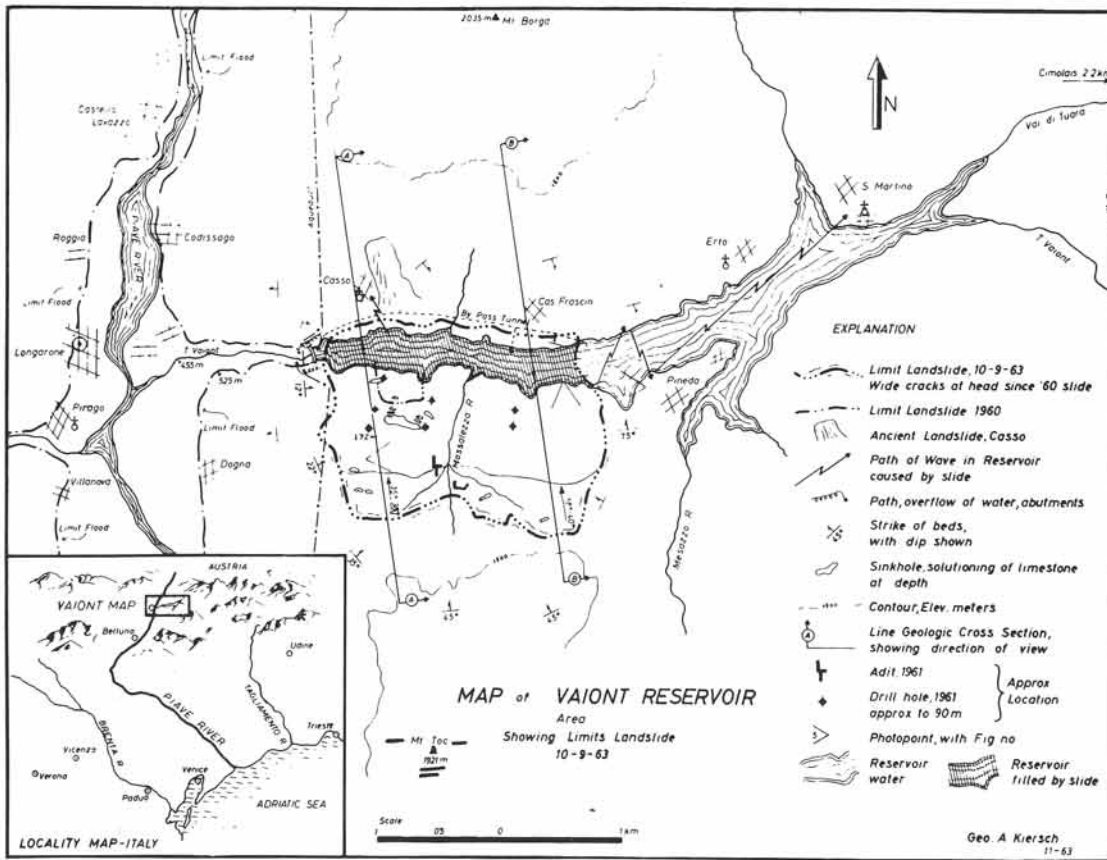


Figure 15-13a: Geotechnical map of the Vaiont reservoir and the extent of the 1963 rockslide.

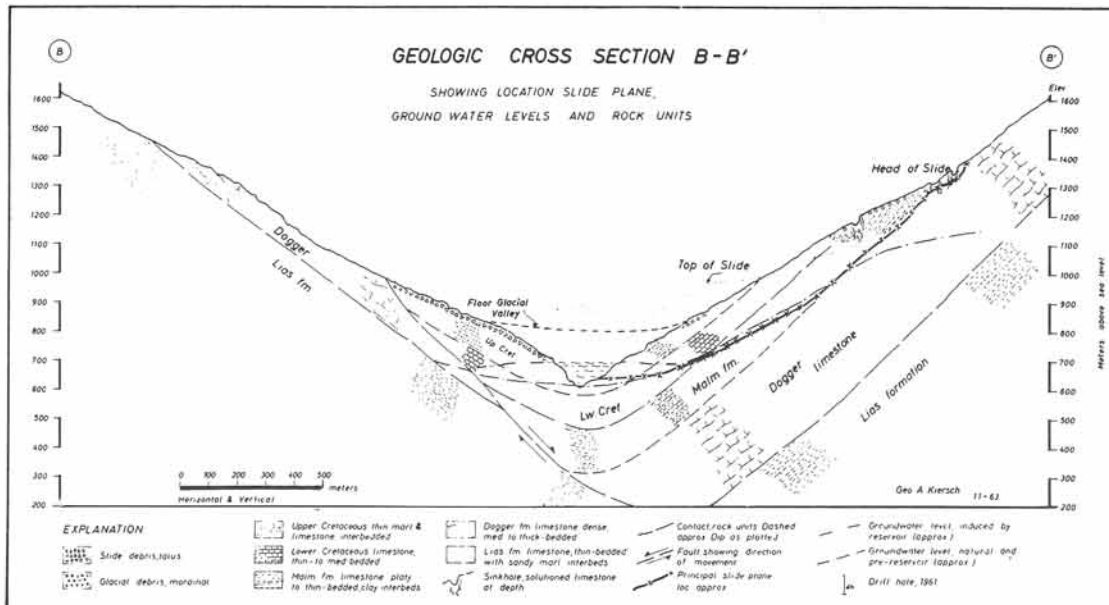


Figure 15-13b: Unstable dip-slopes of stratigraphic bedding, overlying swelling clays, caused the Vaiont slide, Italy, 1963.

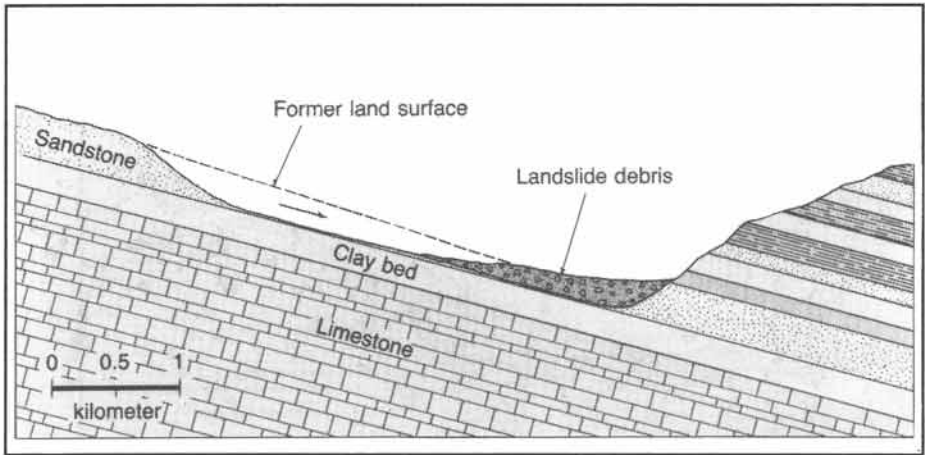


Figure 15-14: Cross-section of the Gros Ventre slide, Wyoming, 1923.

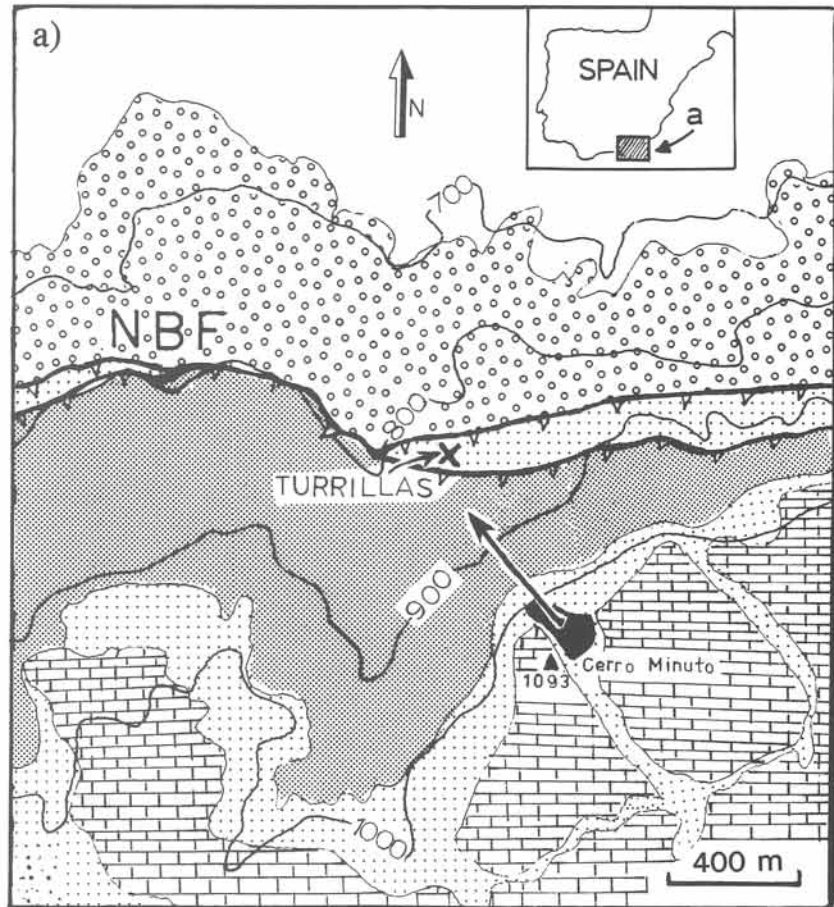
Sierra Alhamilla, Betic Cordillera, Spain. The village of Turrillas is built on top of, at least, four ancient rock slides (Fig. 15-14b). Turrillas is presently located below a potential landslide mass of three million tons of rock included in the unstable Cerro Minuto near the 1093-meter summit above the village. Incipient movement is indicated by open cracks at Cerro Minuto.

Exercise 15-2: The detailed drift map and cross-sections of the Turrillas area are shown in Figure 15-17a & b. a) Color the various slide masses, and estimate the surface area covered by ancient slides. b) Write a summary of the geological history.



Figure 15-15: A classical example of an ancient (prehistoric) debris-flow, recognized as such from its geomorphology of altered volcanic rocks, Pahsimeroi River, South Idaho.

Figure 15-16: Threat of rockslides near Turrillas, southeast Spain. a) Geological outcrop pattern of solid geology on topographic base map. The unstable limestone cliff of Cerro Minuto has a movement trajectory directed at Turrillas village. The Northern Boundary Fault (NBF) separates Tortonian clastics in the north wall from the uplifted metamorphic basement south of the fault. See Figure 15-17a for legend. b) View of Turrillas from Cerro Minuto. Locations 1 to 3 are sites of old rock slides, marked, also, on the drift map of Figure 15-17a.



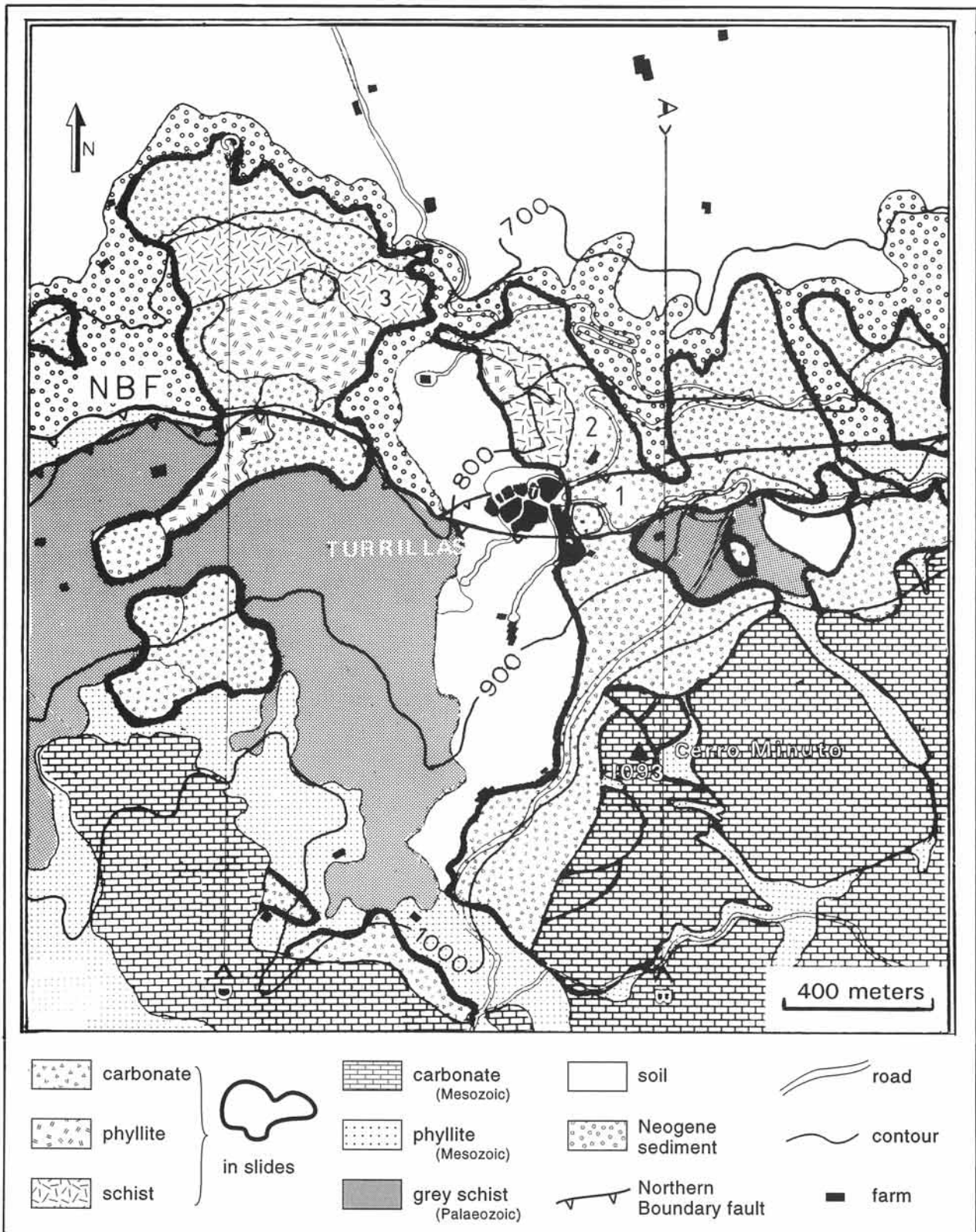


Figure 15-17a: Drift map of the Turrillas area, showing extent of ancient slide masses. Compare with the map of solid geology for the same area in Figure 15-16a.

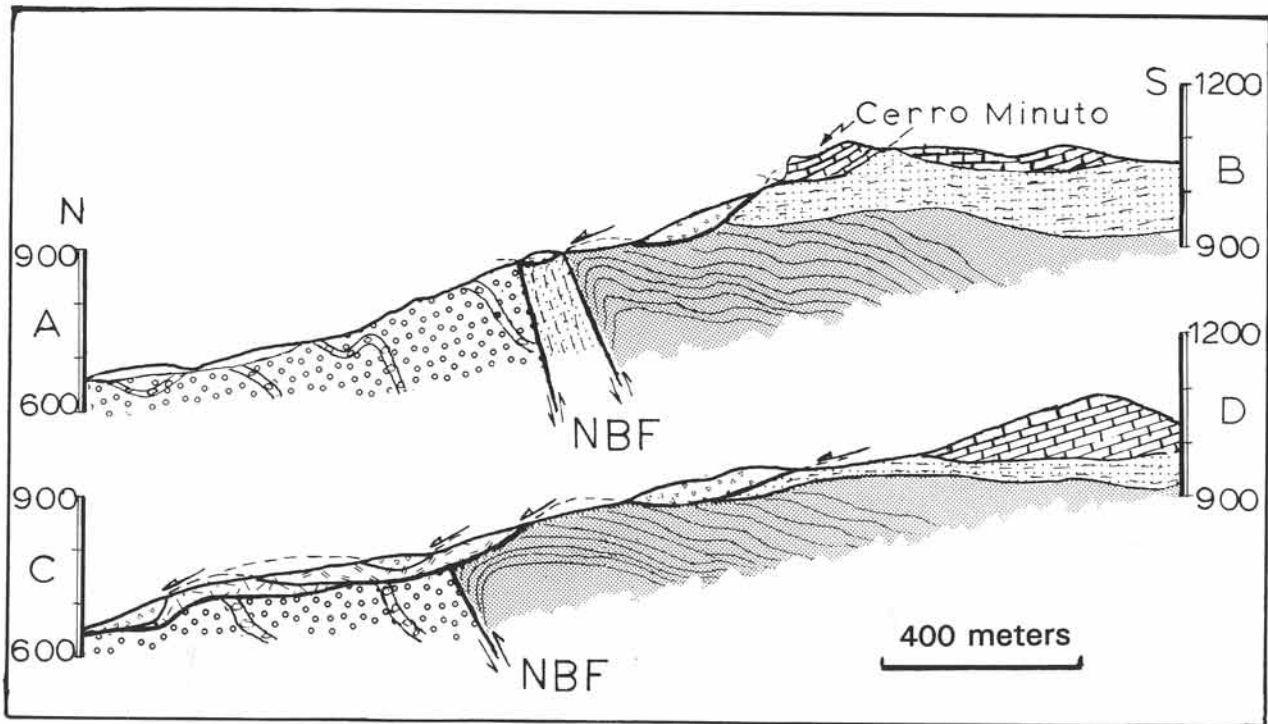


Figure 15-17b: Cross-sections of the Turrillas slides along the locations outlined on Figure 15-17a.

15-3 Sinkholes

Engineering projects may be severely delayed and overrun their budgets if large cavities and caves threaten to destabilize the support of huge construction. For example, the Keban Dam in eastern Anatolia, Turkey, was completed in 1974, three years after its scheduled opening and with enormous cost incurrence (Fig. 15-18). The dam is founded on karstic limestone, underlaid by impervious schist at 345 meters depth. The porous limestone section had to be cut off by a grout curtain and a buried concrete wall down to 345 meters to guarantee a reliable water cut-off. The main cause of the delay in this already ambitious operation was the discovery, during the construction work, of a huge solution cavity 330 meters below the crest of the dam. The cavity, measuring 138 meters long, 117 meters wide, and 30 meters high, was stopped with 60,000 cubic meters of concrete. The superstructure of the dam itself is only 170 meters high.

Solution cavities form in limestone by the solution and transport of calcium carbonate after seepage of corrosive ground water, that is slightly acidic if charged with organic carbon dioxide. The hydrologic circulation pattern may concentrate the corrosive ground water flow in particular fracture zones, but the pattern of solution caves and cavities is commonly chaotic (Fig. 15-19). The presence of solution cavities in the subsurface may sometimes be inferred from the occurrence of *sinkholes* at the surface. These are conspicuous collapse features, forming circular pits in the landscape, termed a *karst topography* if the sinkholes are abundant (Fig. 15-20a). A huge sinkhole in the Manati area, Puerto Rico, is utilized to support the Arecibo deep-space radio telescope (Fig. 15-20b). Pockmarked karst surfaces occur in the Mammoth Cave area, Kentucky; western Texas; Florida; and New Mexico, where the Carlsbad Caverns occur (Fig. 15-21).

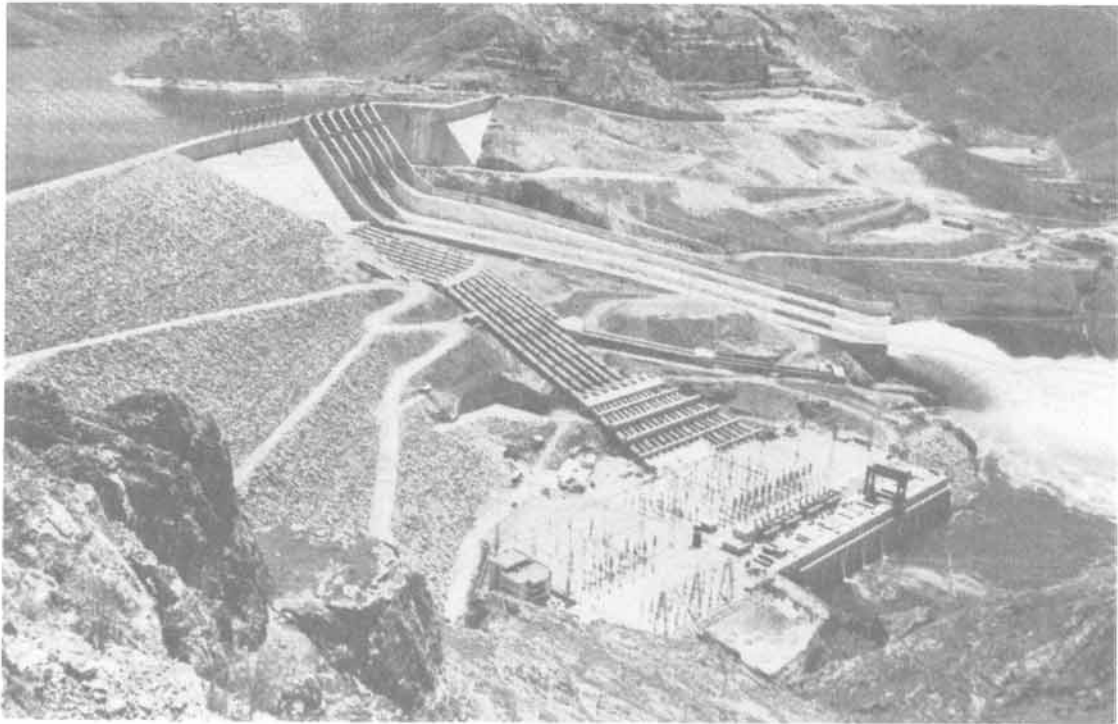


Figure 15-18: Completed Keban hydropower dam, Turkey, which involved stabilization of the dam foundation by works down to 345 meters beneath the surface.

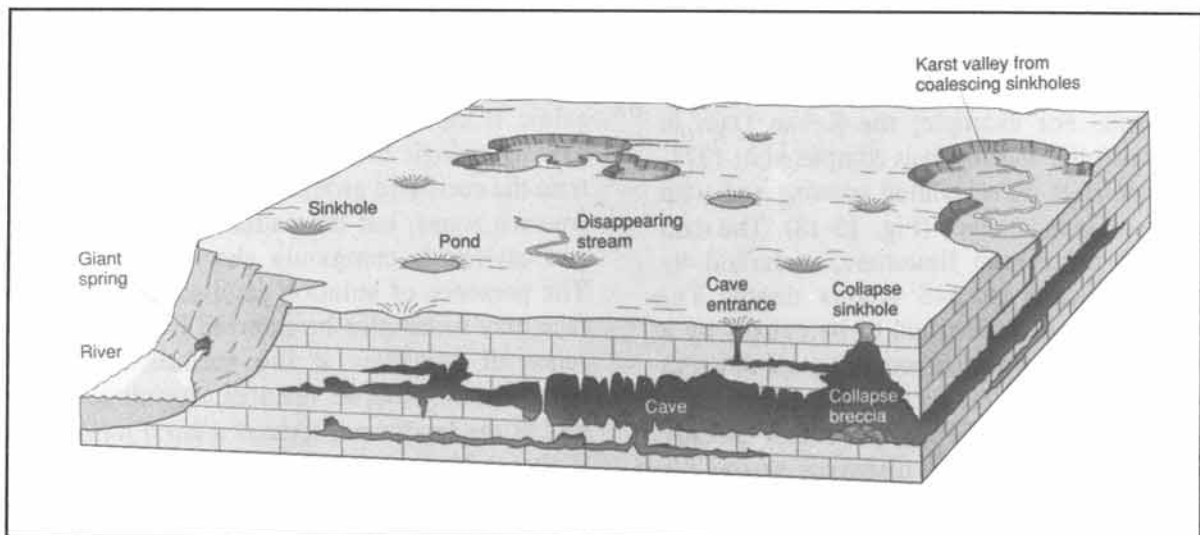


Figure 15-19: Schematic block diagram of a karstic limestone formation with underground caves and surface sinkholes.

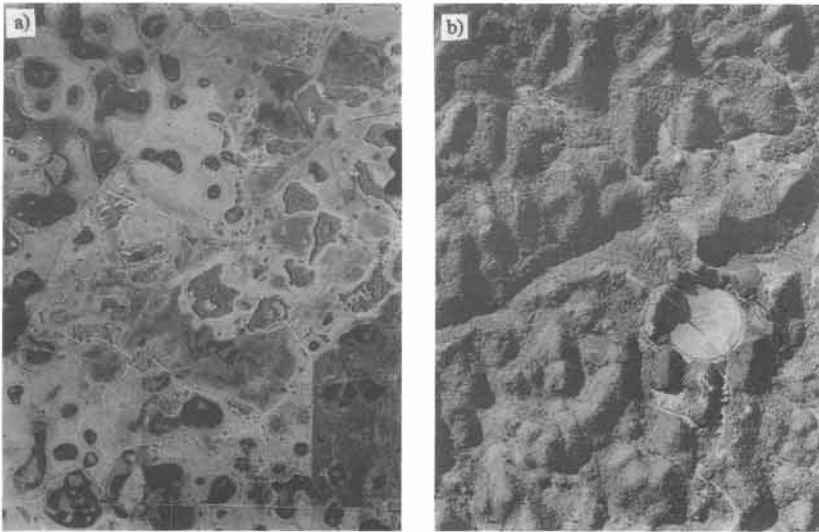


Figure 15-20: Two aerial views of karst landscapes: a) Florida, USA, b) Manati area, Puerto Rico.

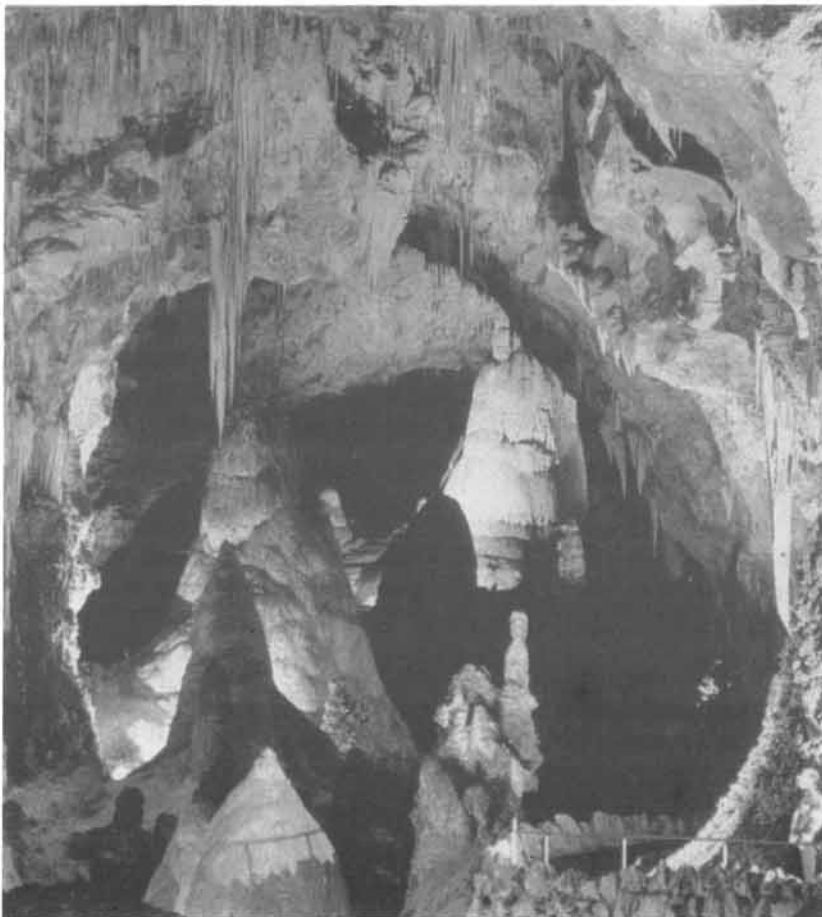


Figure 15-21: Underground solution cave at Carlsbad Caves, New Mexico.

- Exercise 15-3:**
- a) What particular geological hazard threatens the urbanization of a karstic area?
- b) Argue whether it is advisable to use sinkholes for uncontrolled waste disposal.

15-4 Glacial Structures

Huge portions of the continents have been covered by ice sheets during recurrent epochs of glaciation during past ice ages or *glacials*. The geological map pattern of many regions may be obscured by superficial deposits, laid down during past glacials. Ice is a crystalline substance and slowly spreads under its own weight like a drop of oil, but at extremely slow velocity. Nonetheless, any rubble and debris inside and on top of the ice sheets and glaciers is eventually transported to the rim of the ice expanse. Even when the ice masses retreat, we can recognize the former location of their margin because of the rock rubble or *moraines* accumulated in sinuous ridges across the landscape. Figure 15-22 illustrates such an end-moraine and the adjacent ground-moraine, left behind underneath the receding glacier. Beyond the area formerly covered by the glacier is the outwash plain, where glacial melt waters have deposited the mud-fraction or *till*. The outwash plain may feature pockmarks, termed *kettles*, that resemble sinkholes of karstic terrains.

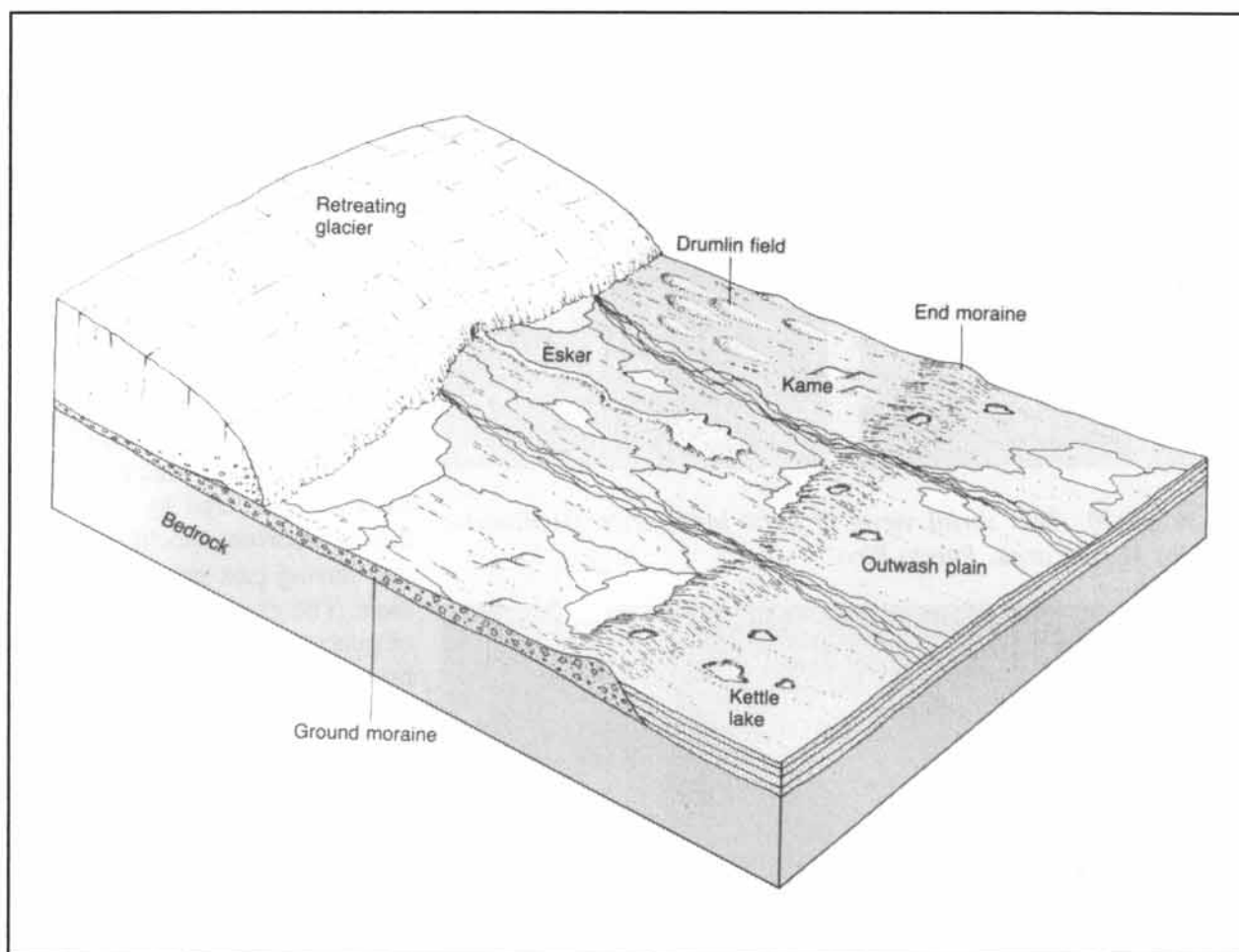


Figure 15-22: Perspective diagram, showing the various superficial deposits left behind by a retreating glacier.

However, kettles and kettle lakes are formed when blocks of ice stick into the till-mud and prevent the accumulation of any tills until they melt, thus leaving a pit or kettle in the outwash plain.

Other depositional patterns, found on the ground-moraine of glaciated terrains, are the eskers, drumlins, and kames. *Eskers* are narrow ridges of sedimentary rock that form in subglacial streams, while their lateral extent is constrained by the subglacial tunnel that holds the melt-water

(Fig. 15-22). Once the glacier retreats, the esker deposits form topographic ridges in the terrain. *Drumlins* range in height from fifteen to fifty meters and occur in groups of parallel, elongated, small hillocks, resembling a group of whales, surfacing in the ocean (Fig. 15-22). It is assumed that drumlins are molded from the unconsolidated deposits beneath an advancing glacier. *Kame* terraces are steep-sided hills, deposited by melt-water in openings within the glacier. They form isolated and irregular mounds.

□ Exercise 15-4: Figure 15-23 illustrates the end-moraines in the Great Lakes region, North America, deposited during the Wisconsinian glacial, that lasted from 150,000 to 10,000 years ago. Distinguish and interconnect the various moraines that mark the different, temporal maximum expansions of the ice front. Were the Wisconsinian end-moraines formed before or after the Illinoian end-moraines?

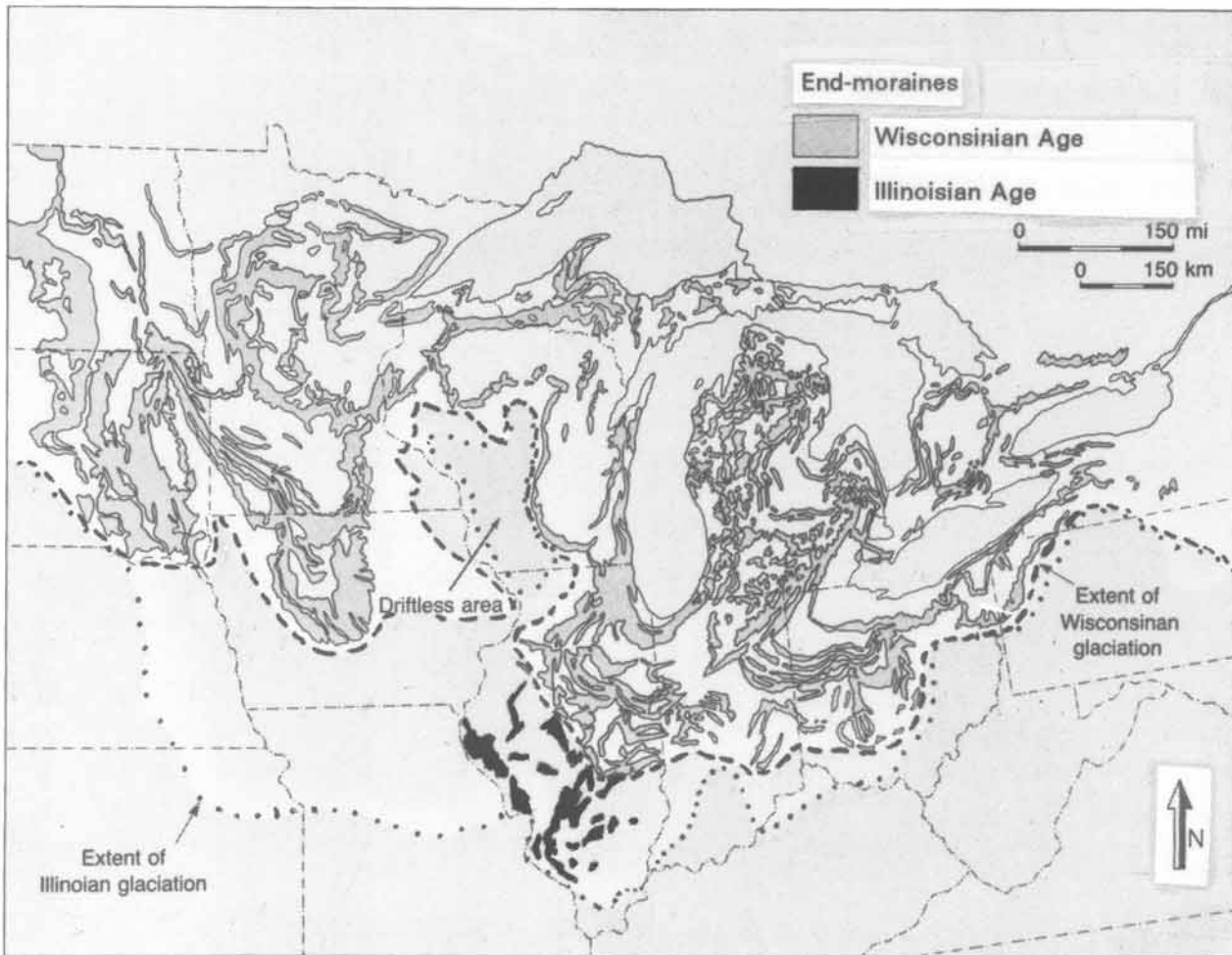


Figure 15-23: Wisconsinian and Illinoian end-moraines in the Great Lakes region, North America.

Chapter 16: Remote-Sensing Maps

MODERN GEOLOGICAL mapping is increasingly supported by a range of high-quality images of the ground surface obtained by various remote sensing devices. Such images give a bird's-eye view of the terrain, are used to map the principal geological features, and are indispensable for planning traverses on the ground. Enlargements may serve as base maps for plotting field data collected on the ground. Remote sensing has evolved into a major discipline within the earth sciences and should be studied in one or more course(s) dedicated exclusively to the subject. This chapter serves as a primer only and outlines some major principles and uses of images obtained by remote-sensing methods. Complementary and fuller coverage of the subject is found in specialist sources, cited in *Appendix A*. Sources of satellite images and aerial photographs are included in the *Additional Resources*.

Contents: The electromagnetic spectrum and its fundamental role in remote sensing are explained in section 16-1. Various platforms for recording electromagnetic radiation are outlined in section 16-2. Principles of aerial photography are discussed in section 16-3. Some methods of photo interpretation are introduced in section 16-4. Several satellite imaging systems, including Landsat and SPOT, are presented in sections 16-5 and 16-6. Digital image processing is briefly introduced in section 16-7. Examples of radar application are provided in section 16-8.

16-1 Electromagnetic spectrum

Taken literally, remote sensing is the observation of an object from a distance without touching the object. In geoscience, remote sensing is restricted to visualization of electromagnetic waves reflected and radiated from the ground surface. Gravity, magnetic, and electrical field

geophysical surveys are beyond the scope of remote sensing as commonly used. Of course, such geophysical data are important for interpreting regional geological subsurface features. However, our attention concentrates on electromagnetic radiation patterns, recorded by a range of remote-sensing methods.

The electromagnetic spectrum consists of a continuum of energy traveling at the speed of light, 300,000 kilometers per second. It can be divided into several spectral bands, covering a particular range of wavelengths. Remote sensing refers to the spectral bands in terms of wave-

lengths, whereas electronic engineers communicate in terms of frequency bands. The relationship between wavelength bands (λ) and frequency (f) is given by the expression:

$$\lambda = c/f \tag{16-1}$$

where c is the velocity of light. Obviously, shorter wavelengths have higher frequencies, and longer wavelengths have lower frequencies.

Figure 16-1 summarizes the major spectral bands of the electromagnetic spectrum used in remote sensing. The photographic band is seen to include light visible to the human eye plus parts of the ultraviolet and reflective infrared spectral bands. The thermal band covers thermal infrared wavelengths. Several radar bands (K, X, and L) are included in the microwave region of the electromagnetic spectrum. Radar is an *active remote sensing system*, transmitting microwave energy to the Earth's surface. The energy interacts with the terrain and is then returned to radar receivers aboard the airplane or spacecraft. In contrast, *passive imaging systems* utilize natural energy from the photographic and thermal infrared bands. These spectral bands receive natural radiation from the Earth's surface. The maximum intensity of natural electromagnetic energy occurs at $0.5\mu\text{m}$ for reflected (sun) light (arrow a, Fig. 16-1) and at $9.7\mu\text{m}$ for thermal infrared energy, radiated at night and during the day (arrow b, Fig. 16-1).

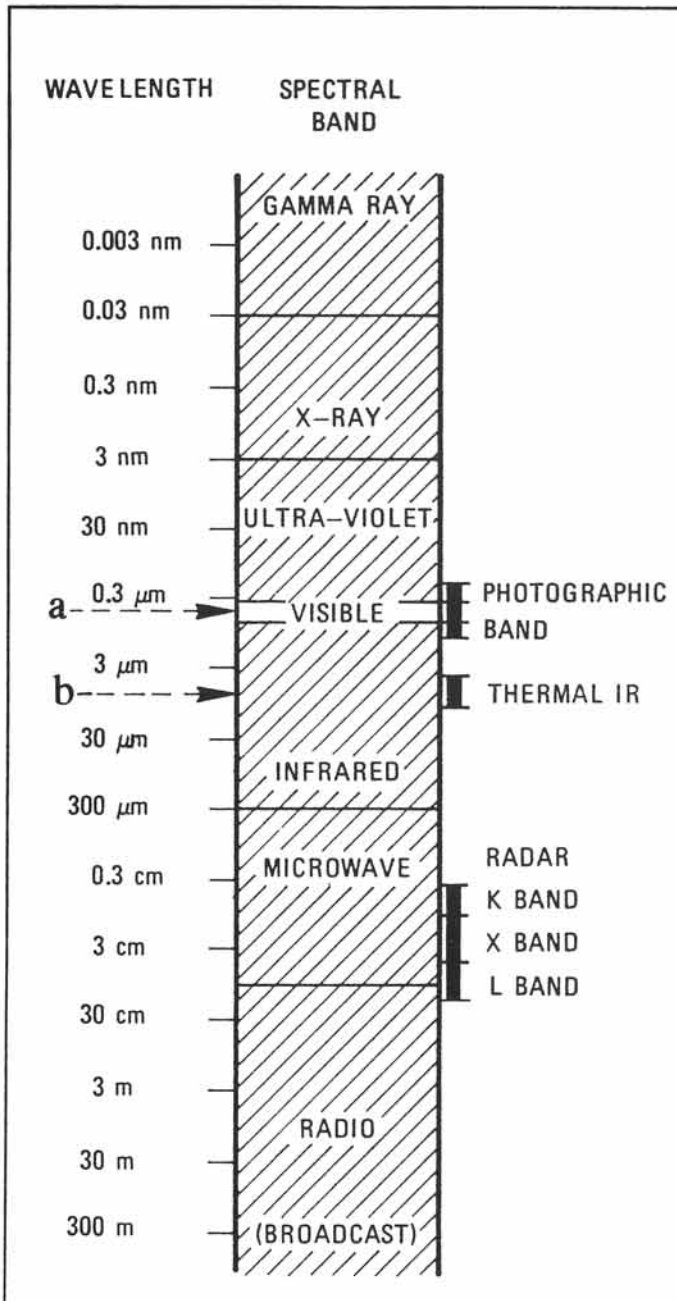


Figure 16-1: Spectral bands of electromagnetic radiation, their corresponding wavelength range, and parts of the spectrum used in remote sensing.

□ Exercise 16-1: Photons may be considered physical particles, involved in the energy transfer of electromagnetic waves, traveling with the speed of light. Calculate the frequency ranges of cycles per second (or Hertz) involved in remote sensing of: (a) visible light (0.4 to $0.7\mu\text{m}$), (b) thermal infrared waves (1.3 to $14\mu\text{m}$), and (c) radarwaves (K-, X-, and L-bands between 0.8 and 30cm).

16-2 Data collection

Photographs from the Earth's surface have been gathered since about 1850, using a range of vehicles: balloons, kites, pigeons, aircraft, rockets, and space probes. Classical aerial photography records images of electromagnetic radiation by means of chemicals on film. It was first widely used in aerial surveys for military intelligence operations during the First World War. Most aerial surveys detect visible light only, the most common form of electromagnetic energy, occupying wavelengths between 0.4 and 0.7 μm . But portions of the adjacent UV-band (0.3 to 0.4 μm) and reflective IR-bands (0.7 to 0.9 μm) can, also, be utilized in conventional photography, provided that special film and filters are used.

Starting in the 1960's, technological advances of electromagnetic sensors, radio transmission, and computer technology allowed the color visualization of wavelength patterns in images of spectral bands other than that of visible light only. The data are commonly recorded in digital format, and an array of image-processing techniques allows visualization and enhancement of particular patterns in the monitored wavelength. Stored in a computer, they can be retrieved and processed at space imagery rectification centers into a wide variety of maps and images. The resulting images utilize gray scales and true or false colors to highlight contrasts in the recorded electromagnetic radiation.

Among the most common forms of modern satellite imaging data available to the general public are: Landsat, SPOT, Metric Camera, Large Format Camera, and KFA-100. Table 16-1 compares their scales of resolution and area coverage with that of conventional, low-altitude photographs. The resolution is the minimum length scale required for an object on the ground to become visible. The resolution of conventional photographs is still up to a hundred times better than that of any digital satellite image. More specifically, the most expensive techniques (Land-

Table 16-1: Altitude, frame size, and image resolution of some remote sensing platforms.

Platform	Technique	Oper.	Height (km)	Width (km)	Resol (m)
Landsat	multispectral	USA	920	185x185	80
	thematic mapper	USA	920	185x185	30
SPOT	multispectral	Fr	822	60x60	20
	panchromatic	Fr	822	60x60	10
Spacelab	Metric Camera	Ger	250	190x190	20
	Large Fm Cam	USA	250	700x700	8
	KFA-100	Russ	250	75x75	5
Airplane	low altitude photography	many	4	7x7	.3

sat and SPOT) have only moderate resolution (12 to 79 m). Nonetheless, the electronically enhanced Landsat and SPOT images are versatile and commonly yield geological information not visible on aerial photographs. One major advantage of Landsat images is that areas of 185 by 185 km are covered by a single image, allowing a synoptic overview of the region. Typical conventional aerial photographs cover only about 7 by 7 km each, so that many pictures are required to cover larger regions, and, thereby, major tectonic features may not be noticed.

Exercise 16-2: a) Compare and discuss some of the benefits and limitations of both satellite images and aerial photographs for geological mapping purposes. b) Also, compare the limitations and advantages of mapping by remote-sensing methods alone, with those occurring when the geological mapping is done exclusively by observations on the ground by a field geologist.

Exercise 16-3: Several remote-sensing images have appeared in previous chapters. Prepare a list of these remote-sensing images and photographs and specify which type of imagery was used.

16-3 Aerial photography

Aerial photographs are used for making and updating topographic contour-maps, monitoring land use, and serving as base maps for geological mapping. The potential benefits of aerial photographic studies to geologists are considerable. The photos help them to trace the boundaries between major rock units, to locate major folds, faults, joint patterns, karst or sinkholes, and other geological features. The extent of any superficial

cover and distribution of good exposures of the bedrock can be quickly assessed. The accessibility of the terrain and proximity of interesting ground locations to roads and river beds can, also, be examined to prepare a detailed plan for an effective ground survey.

For any area of interest, there may be photographs available at different resolutions and scales, for different years and seasons, and from pictures taken with a variety of cameras and films. Study, and if necessary order, aerial photographs or satellite images (or both) of your prospective field area. Check what is available and what is best suited for your particular application. Before going into the field, prepare a photo-interpretation map and summarize your conclusions in a concise, written report. Aerial photographs are commonly available from various government and private agencies (see *Additional Resources*).

The resolving power of photographic film is exceptionally good compared to other forms of remote sensing (Table 16-1). Table 16-2 summarizes the minimum ground separation ($R_g/2$) on airphotos for a range of flight altitudes. The ground resolution (R_g) is obviously influenced by the system resolution, which resides in the quality of the camera and film. Table 16-2 uses two examples with resolutions of 40 line-pairs per mm and 100 line-pairs per mm, respectively. Table 16-3 lists the minimum ground separation required to recognize particular features. Rivers, urbanized and cultivated areas, and roadways can be easily recognized on aerial photographs. Likewise, a range of geological boundaries may be distinguished, based upon geological experience and expertise (section 16-4).

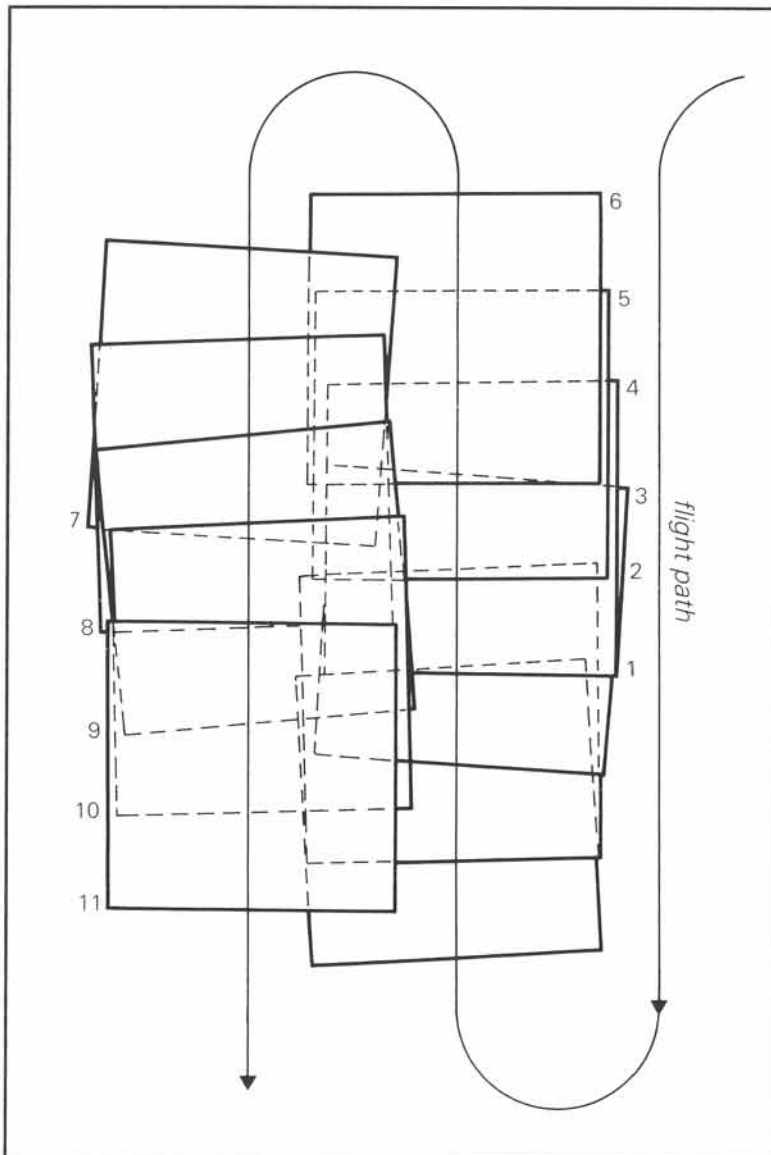


Figure 16-2: The arrangement of individual photographs in an aerial survey is determined by the flight path of the aircraft.

Table 16-2: Ground separation limit on classical aerial photographs, for various standard scales.

Altitude (m)	Scale	Ground separation for line pairs/mm	
		40 (m)	100 (m)
6,100	1:40,000	0.5	0.2
4,575	1:30,000	0.37	0.15
3,050	1:20,000	0.25	0.1
1,525	1:10,000	0.12	0.05

Table 16-3: Features identifiable on aerial photographs of various ground separation limits.

Ground separation (m)	Features identifiable
15	Rivers, mountains, and lakes
4.5	Cultivation parcels
1.5	Roads
0.15	Automobiles
0.05	Individual trees and people counts



Figure 16-3: Mosaic of high altitude aerial photographs of Dammam Dome at the Arabian Gulf, Saudi Arabia. This area shown in photomosaic is about thirty kilometers in width.

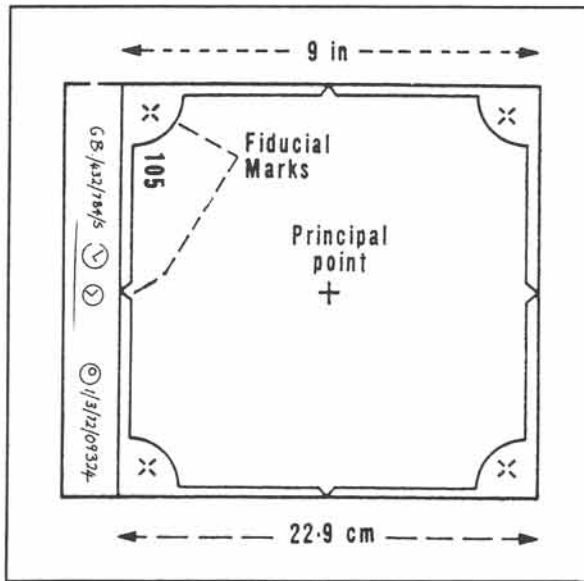


Figure 16-4: Standard aerial photograph with fiducial marks (crosses) and flight data.

Aerial photographs are commonly made from aircraft that fly parallel flight-paths or runs (Fig. 16-2). The frames within each run are spaced to ensure mutual overlap of about 60 percent between successive frames. There is, also, some 10 percent sidelap with the photographs of adjacent

runs. Because each photograph covers only a limited area, tens to hundreds of photos are commonly needed to cover the ground for a regional survey. In order to locate the relative position of the pictures, a coverage diagram or index map is usually available from the agency supplying the prints. A print laydown or photo-mosaic, where the images are laid down in their approximate geographic location with serial numbers visible, is, also, very practical to keep track of the relative position of aerial photographs (Fig. 16-3). Small deviations from the planned flight path, due to variations in wind speed and direction, as well as thermal airflows, result in misalignment and slight rotation of adjacent photographs.

Each photograph is marked with flight numbers, serial numbers, flying altitude of the plane, focal length of the camera lens, date of photography and country represented (Fig. 16-4). The center or principal point of each photograph may be found at the intersection of each connecting fiducial mark at the margins of the frame. Overlapping photographs may be used to simulate a stereoscopic view or model of the terrain. Two images with considerable overlap, a so-called

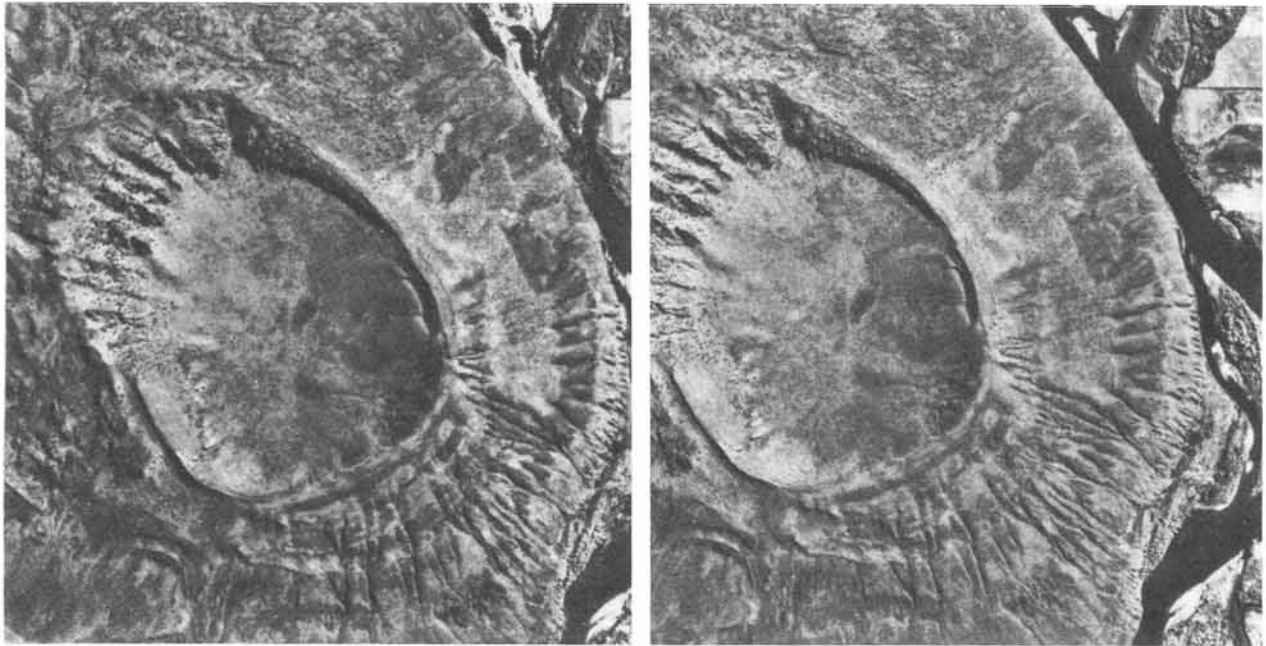


Figure 16-5: Stereopair of Menan Buttes volcano, Idaho, USA. Image width is about 1.5 km.



Figure 16-6a: Stereoscope is used to create virtual-reality images of landscape from a stereopair of aerial photographs.

stereopair, are laid down in a horizontal row. Only overlapping areas can create stereo vision, and it is important that these areas are similarly oriented with eye-base parallel to the flight line in each of the stereopairs studied. Figure 16-5 is a stereopair (showing only the cropped and overlapping portions of two adjacent aerial photographs) of the Menan Buttes volcano in southern Idaho, USA. The frame is 1.5 kilometers wide.

The illusion of a three-dimensional model of the landscape is created using a stereoscope (Fig. 16-6a). This is an optical device of various design, which aids the left and right eyes to merge the images of the left and right photographs into one stereoscopic view. The brain produces a three-dimensional view of the landscape, as seen directly from above at the time of the flight. Generally, there is a vertical exaggeration of two to four times the horizontal scale, which greatly aids geological interpretation and dip-strike estimation. With a little practice, and after adjusting the lens separation and photo positions, stereoscopic viewing becomes a powerful tool to examine the terrain in a bird's-eye view.



Figure 16-6b: Geologists make interpretation maps of aerial photographs on transparent overlays.

□ **Exercise 16-4:** A standard size of aerial photographic prints measures 22.9 by 22.9 cm (9 by 9 inches). Consider three common scales used, 1:60,000, 1:40,000, and 1:30,000, and calculate for each scale the dimensions of the corresponding ground area.

16-4 Photo interpretation

The aerial photograph reduces the ground surface to a scale that can be managed and analyzed in desk studies. A careful photogeology study closely examines the vast amount of data recorded on the images. The image shows variations in tone, texture, relief, size, and shape, as well as an inventory of the spatial distribution of surface features. The viewpoint provided in aerial images is unique and complementary to ground-based observations.

The study of aerial photographs can be done either with or without the use of stereopairs.

Experienced users may find they can do well without stereo enhancement, and the interpretation is done directly onto a single photograph. The very fine grain and large format film used in aerial photography sustain enlargements, if so required, without any significant quality loss. Even photostat copies and enlargements of good quality originals may provide useful bases for photo interpretations. The actual interpretations are traditionally done onto overlays of transparent tracing paper (Fig. 16-6b). Alternatively, analog aerial photographs can be scanned into digital format and interpretations can be traced on the computer screen, if so required. A relatively new trend in aerial photography is to use digital,

rather than analog, cameras, so that advanced image processing is possible after acquiring the digital image files without need for scanning.

The information on aerial photographs is usually recorded in gray tones of the black and white scale. The photograph records the light reflected by the ground surface. The ratio of reflected energy to incident energy is called the albedo. Dark surfaces have low albedos, and light surfaces have high albedos. The tone of the image is affected, not only by the nature of the surface photographed, but also by such factors as atmospheric conditions, solar position, film properties, flight schedule, and camera performance.



Figure 16-7: Oblique aerial view of inclined sedimentary beds. Dip is to the left. Road for scale.

The photographic appearance of the terrain is, also, affected by vegetation, drainage patterns, soil cover, jointing, weathering, erosion rates, rock composition, deformation structures, and other geological features, such as karsting, bedding and volcanism. Another feature affecting photo interpretation is the topographic relief of the terrain. It should be kept in mind that all slopes of both bedding and any topographic relief often appear much steeper in the stereoview than in reality. However, vertical exaggeration is usually a desirable artifact of the stereoscopic set-up. The direction of dip of layers can be inferred from the V-shaped intersection, where geological boundaries are cut by major valleys. Generally, the V-pattern points down-dip where beds cross stream-channels. Figure 16-7 is an oblique aerial photograph of uniformly dipping sedimentary strata with a geomorphology defined by linear ridges and flat-tops of dip-slopes, transected by a parallel drainage pattern. Patterns of drainage networks can take on many distinct forms, often related to the underlying geology. A regional plateau, made up of horizontal strata, may be transected by meandering rivers (Fig. 16-8). Other basic drainage patterns are illustrated in

Figure 16-9a to f. Many more variations and combinations of drainage patterns are found in nature, but nearly all may be related to the basic patterns shown.

In spite of the variability in tone, comparison of the relative tonal values within an image may help to distinguish rock units. Rocks composed of mafic minerals tend to absorb much radiation and appear with dark tones on the image (gabbros, basalts, and amphibolites). Rocks of felsic minerals and evaporites tend to appear as light tones on the image (granites, sandstones, and carbonates). Intermediate tones are produced by diorites, shales, slates, and schists. Water in rivers, lakes, and seas absorbs radiation and, therefore, has a dark tone on aerial photographs. In addition to tone and texture, shape and size may help to differentiate further between rock units. For example, intrusive bodies of granite, diorite, and

gabbro are all likely to be subcircular with diameters ranging between one to ten kilometers. Intrusive bodies are typically transected by joint patterns, which commonly control the drainage network into rectangular and trellis patterns. Sedimentary rocks are typically layered and include boundaries with sharp tonal contrasts. Carbonates may be distinguished from sandstone units by the presence of sinkholes. Metamorphic rocks are typically foliated but have fewer sharp tonal or color contrasts, due to the homogenizing effect of mineralogical changes induced by metamorphism.

A photogeological interpretation can progress systematically, following the hints given below: (1) Assess the nature and extent of vegetation, together with the climatic environment (humid, arid, temperate, or tropical). (2) Describe the topography of the terrain, geomorphology, and



Figure 16-8: Low-altitude, oblique aerial photograph of a terrain made up of horizontally bedded sedimentary rocks, transected by a meandering river, USA.

type of drainage pattern. (3) Mention any major culture and settlement centers. (4) Decide what erosional agent is dominant in the area studied (wind, ice, water). Before proceeding, use a transparent overlay on top of the photograph to draw a geological interpretation map. Start your map by drawing a frame around the area, include a scale bar and north arrow, and mark the map with photo fiducial marks and serial numbers, together with a suitable name for the area studied. Then proceed as follows: (5) Divide the region into areas covered by surficial deposits, and outline the major exposures. (6) Establish the nature of the bedrock (sedimentary, metamorphic,

or igneous rocks). (7) Trace the boundaries between the major rock units. (8) Include structural symbols on the map for strike and dip of strata, mark traces of faults and fold axes, indicate antiforms, synforms, and sense of movement on faults. Common symbols used on the interpretation maps of remote-sensing images are given in Figure 16-10. (9) Include a legend with your photo-interpretation map. (10) Consider the geological history of the area. (11) Write an outline to accompany your map, addressing the topics and features mentioned under points 1 to 10.

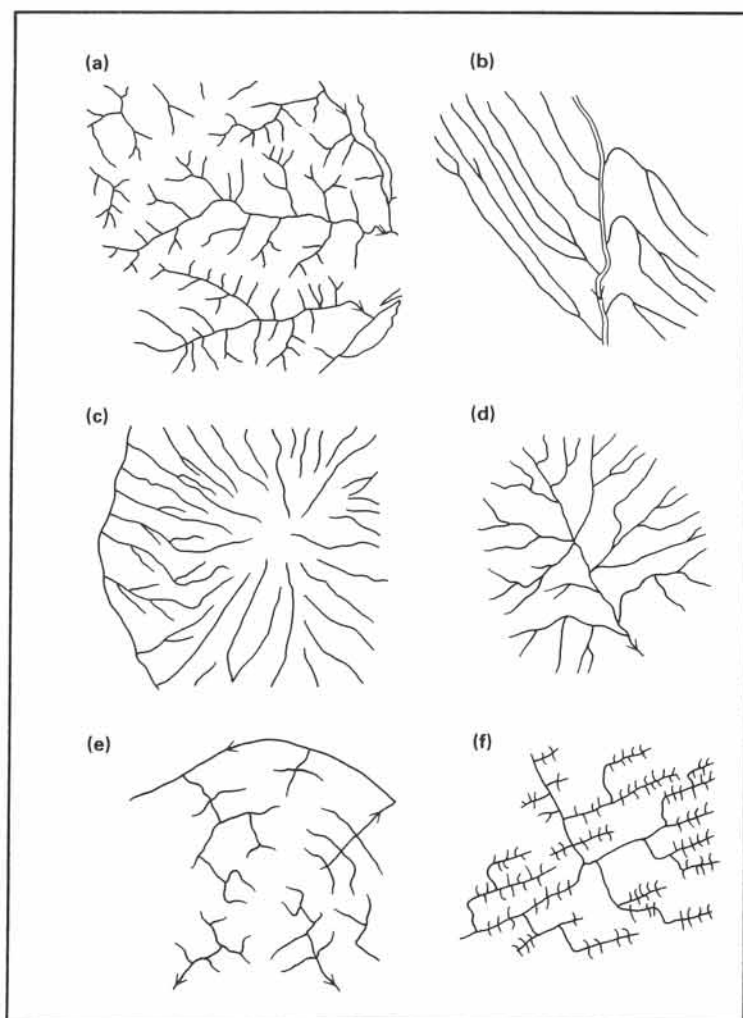


Figure 16-9: Basic forms of drainage patterns: (a) dendritic, (b) parallel, (c) radial, (d) centripetal, (e) annular, and (f) trellis.

Some examples of aerial photographs of different terrains are shown in Figures 16-11 to 16-14. Figure 16-11 is a stereopair of vertical aerial photographs showing *barchan dunes* in the Californian Mojave Desert. Figure 16-12 is a stereopair of vertical airphotos of folded strata in Wyoming, USA. Figure 16-13 is a stereopair of the Precambrian shield of western Saudi Arabia. The area comprises granitic intrusions and foliated supracrustals (schists), transected by basic dikes and fault off-sets. Figure 16-14 is a stereopair of Tertiary flood basalt, erupted onto eroded Precambrian basement of the Arabian shield. Visible are basic feeder dikes, transecting jointed plutons and foliated supracrustals of the basement.

□ **Exercise 16-5:** Make photo-geologic interpretation maps of the areas in Figure 16-11 to 16-14. Accompany each map with a written outline, discussing the items of points 1 to 10, mentioned in section 16-4.












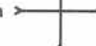







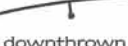
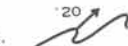

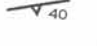



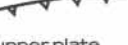
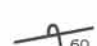
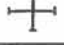
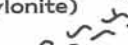
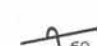



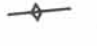



CONTACTS		FAULTS			
<p>Exposed Contact</p> 	<p>Approximate Contact Not surely located within 1/25 inch at scale of map.</p> 	<p>Same line conventions are used for faults as for contacts.</p>			
<p>Inferred Contact Insufficient data to establish contact, but contact must be present. Continuous change from one lithology or rock type to another. Contact arbitrary.</p> 	<p>Concealed Contact Beneath mapped geologic unit, water, or ice.</p> 	<p>Fault, Showing Dip</p> 	<p>Probable or Doubtful Fault Queries, spaced three or more dashes apart, indicate uncertainty of existence, not location.</p> 		
FOLDS					
<p>Same line conventions used as for contacts.</p>		<p>Asymmetric Syncline Showing dip of limbs and direction of plunge.</p> 			
<p>Anticline Showing crestline and direction of plunge.</p> 	<p>Overturned Syncline Showing direction of dip of limbs and plunge.</p> 	<p>Fault Showing Bearing and Plunge of Grooves, Striations, or Slickensides</p> 			
<p>Assymmetric Anticline Showing dip of limbs and plunge.</p> 	<p>Basin</p> 	<p>High-Angle Fault Showing dip; U, upthrown side; D, downthrown side.</p> 			
<p>Overturned Anticline Showing direction of dip of limbs and plunge.</p> 	<th colspan="2">MINOR FOLD AXES</th>		MINOR FOLD AXES		
<p>Dome Generally used on small scale, tectonic maps only.</p> 	<p>Minor Anticline Showing plunge.</p> 	<p>Strike Slip Fault Fault showing relative horizontal movement.</p> 			
<p>Syncline Showing troughline and direction of plunge.</p> 	<p>Minor Syncline Showing plunge.</p> 	<p>High-Angle Fault Bar and ball are on the downthrown side.</p> 			
<th colspan="4">PLANAR FEATURES</th>		PLANAR FEATURES			
<p>Planar symbols (strike and dip of beds, foliation or schistosity, and cleavage).</p>		<p>Minor Folds Showing plunge of axes. Used where beds are too tightly folded to show axes of individual folds separately.</p> 			
<p>BEDDING</p>		<p>CLEAVAGE</p>			
<p>Strike and Dip of Beds</p> 	<p>Strike and Dip of Cleavage</p> 	<p>Reverse Fault R, upthrown side; angle of dip originally greater than 45 degrees.</p> 			
<p>Strike and Dip of Beds Top of beds known from sedimentary features.</p> 	<p>Strike of Vertical Cleavage</p> 	<p>Thrust Fault Sawteeth are on the upper plate.</p> 			
<p>Strike and Dip of Overturned Beds Horizontal beds.</p> 	<p>Horizontal Cleavage</p> 	<p>Fault (Shear or Mylonite) Zone Showing dip.</p> 			
<p>Strike and Dip of Overturned Beds Top of beds known.</p> 	<p>FOLIATION OR SCHISTOSITY</p>	<p>Fault Breccia</p> 			
<p>Strike of Vertical Beds Crumpled, plicated, crenulated, or undulatory beds and beds of average dip.</p> 	<p>Strike and Dip of Foliation</p> 	<p>LINEAR FEATURES May be combined with the above planar symbols as shown.</p>			
<p>Strike of Vertical Foliation</p> 		<p>Bearing and Plunge of Lination</p> 			
<p>Horizontal Foliation</p> 		<p>Vertical Lination</p> 			

Figure 16-10: Symbols suitable for use on photo interpretation maps. However, symbols are not standardized, and many different symbols are in use throughout the world.



Figure 16-11: Stereopair of sand dunes, Mojave Desert, California. Image width is about 1.5 kilometers.



Figure 16-12: Folded sequence. Image width is about two kilometers.

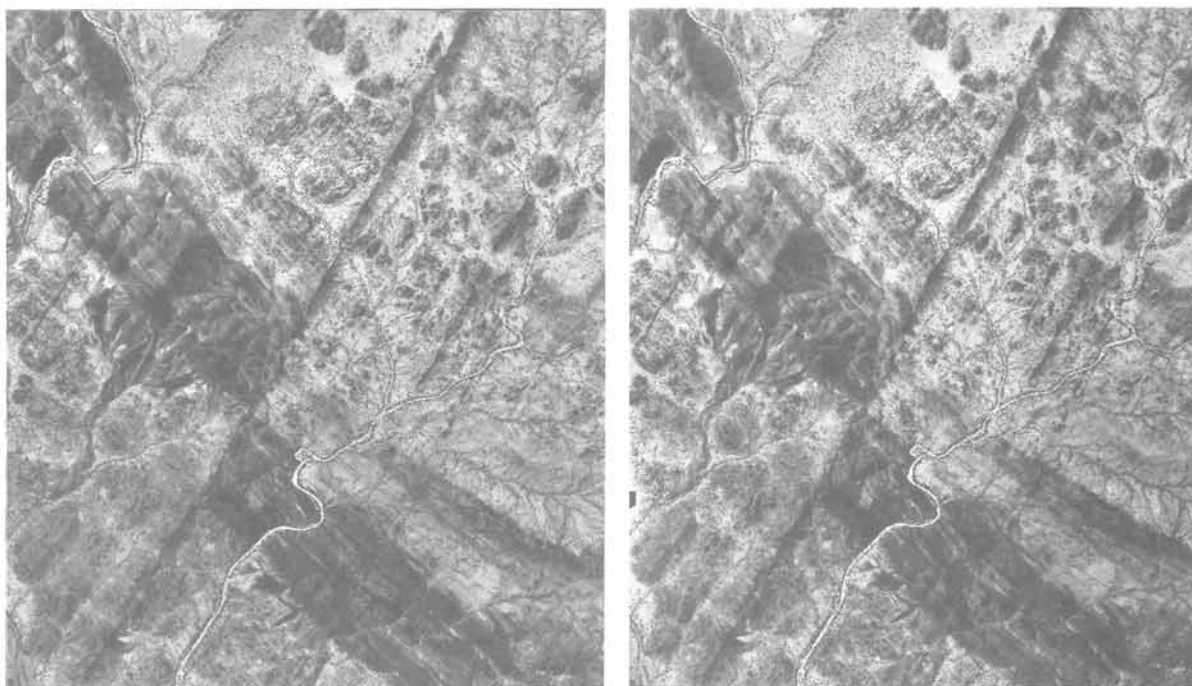


Figure 16-13: Stereopair of fractured supracrustals and igneous basement. Basic dikes intrude the fractures parallel to the fault. Image width is about four kilometers.

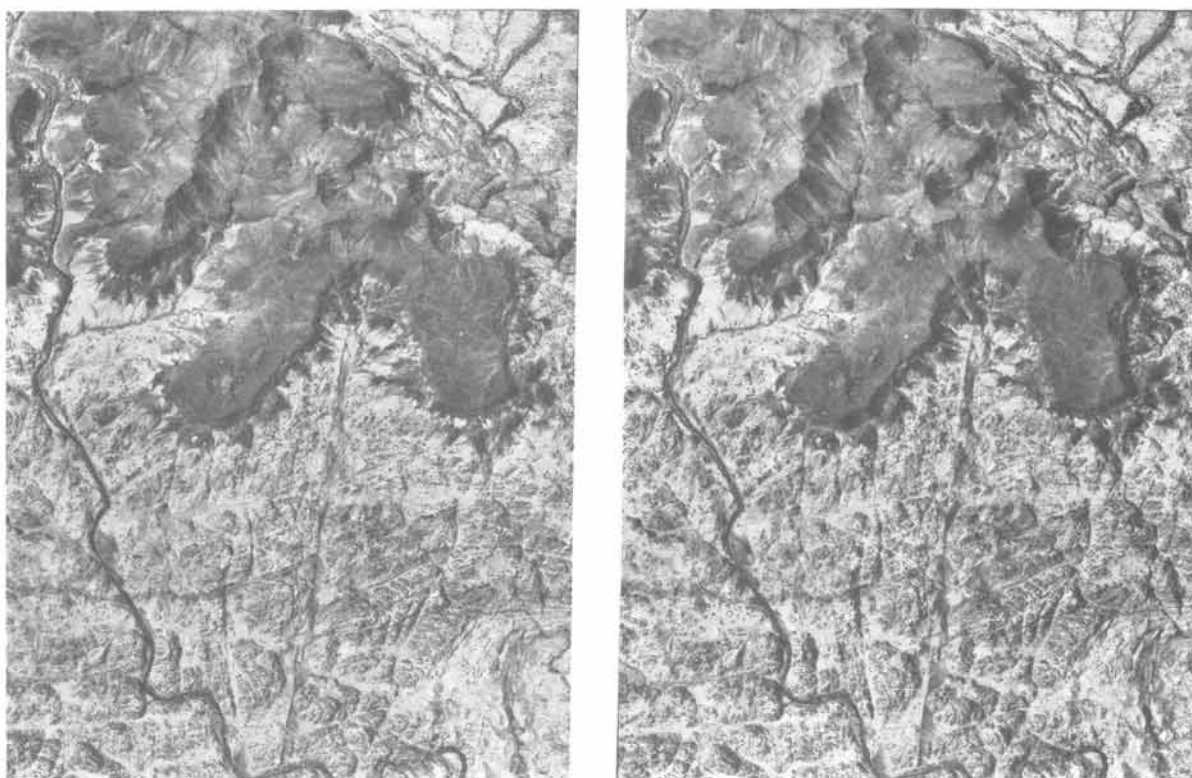


Figure 16-14: Stereopair of Tertiary plateau basalt, resting on Precambrian basement rocks of the Arabian shield. Image width is about 2.5 kilometers.

16-5 Satellite images

Satellite images have a number of advantages over classical aerial photographs. They cover much larger areas, they allow coverage of areas with inaccessible air space, and they are routinely collected and updated by space agencies and, therefore, can be ordered on demand without loss of time. Radial distortion, a problem when making maps from airphotos, is not present on Landsat and SPOT images. Modern satellite images are recorded digitally. Consequently, they can be processed with the aid of sophisticated software to enhance particular features in the image by introducing color coding, and by the shifting and filtering of wavelengths.

More recently, satellite imagery is promoting a technology called Quantitative Structural Mapping (QSM). The idea is to create maps using data from satellites, rather than measurements on the ground, principally because detailed ground-based studies are costly and time-consuming. Obviously, one of the strengths of remote sensing is that it gives instantaneous access to any place in the world. No permission is required to enter the terrain, and cumbersome ground logistics are

Table 16-4: Selection of satellite based remote sensing imagery systems.

Satellite	Scene size (km)	Resolution (m)	Bands
Landsat MSS	185x185	79	four
Landsat TMS	185x185	30	seven
SPOT	60x60	20-10	four

	Swath width (km)	Resolution (m)	Bands
Tiros	2,100	1,100	five
Nimbus	1,600	825	six
HCMM	715	600	two
Seasat	100	25	one

avoided. Digital elevation data from satellite probes can be merged with electromagnetic radiation data to produce detailed perspective views of a terrain (Fig. 16-15). In such images the terrain can be coded, such as to outline boundaries between rock units, faultlines, fold axes, and strike and dip of bedding. Remote sensing, thus, helps to determine the overall structural grain and major lithological subdivisions. Although being a powerful high-tech aid to mapping work, QSM is unlikely to replace geolo-

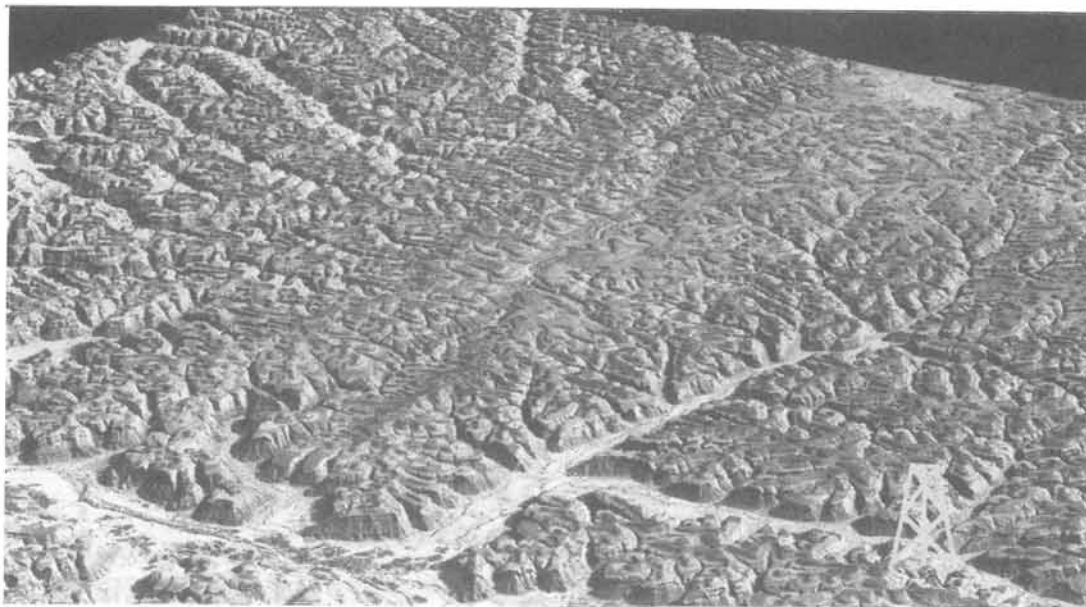


Figure 16-15: Digital animation of landscape in Yemen. Surface geology can be included in the original image by projecting satellite imagery onto the land surface.

gical field work altogether. But it has already been applied successfully in petroleum exploration programs of remote, arid regions.

Returning to our discussion of basic satellite imagery, many different satellites have been launched to collect electromagnetic radiation scans of the ground surface (Table 16-4). Some of these satellites were launched principally for monitoring oceanic currents, sea floor bathymetry, and weather patterns. Their images cover very large areas, but with low resolution. The resolution of some satellites is so low that no detailed geological observations can be made. For example, ground resolution of Tiros, Nimbus, and HCMM is 1,100, 825 and 600 meters, respectively. Seasat records microwaves of 23.5 cm wavelength and maps the bathymetry and tectonics of the sea floor by determining lateral changes of sea-level. However, it reveals little ground contrast, rendering it largely unsuitable for geological studies of continental areas.

The Gemini and Apollo NASA missions of the 1960's included manned spacecraft, which collected satellite images of the Earth's surface with handheld cameras. But most modern, unmanned spacecraft collect images by electromagnetic sensors, mostly with line-scanning techniques. The forward motion of the Landsat spacecraft allows successive elements of the ground to be scanned by detectors of electromagnetic radiation (Fig. 16-16). The scanner is in a fixed position inside the spacecraft and receives electromagnetic radiation via a scan mirror, sweeping back and forth to cover a particular width of the terrain below. The mirror reflects the radiation onto arrays of detectors, transforming the radiation

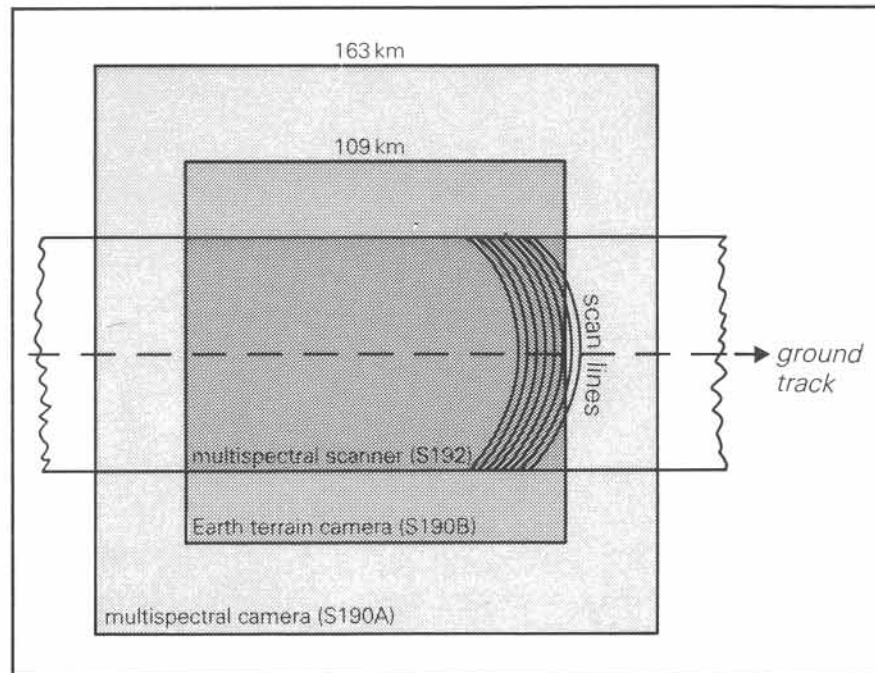


Figure 16-16: Ground track, swath width, and movement of scan lines in different imaging devices.

into a digital signal. The radiation collected by the sensors is usually filtered and differentiated into bands of the visible and infrared wavebands. The ground is covered in sweeps perpendicular to the flight motion and at a rate matching the ground speed, thus ensuring complete coverage of each swath.

Exercise 16-6: The United States can be covered completely by approximately five hundred Landsat images. a) Estimate how many SPOT images are required to cover the same area. b) How many conventional aerial photographs are required?

16-6 Landsat and SPOT images

The best ground resolution in satellite images, available to the public, is presently provided by Landsat thematic mapper and SPOT images. Various generations of Landsat spacecraft, the first of which was launched by NASA in 1972, have collected multispectral scanner images

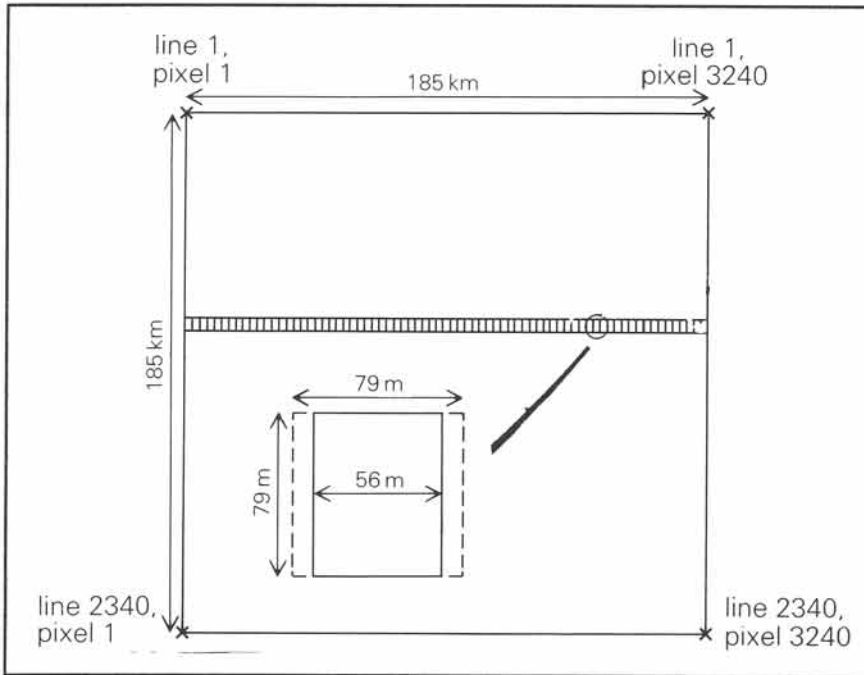


Figure 16-17: Pixel arrangement and size in Landsat MSS images.

(MSS) and, more recently, thematic mapper images (TM). Careful study of satellite images reveals that they are constituted by a pattern of regular lines and columns made up of pixels or picture elements. Each pixel displays either a gray tone or a particular color. For example, each MSS Landsat image is composed of 2340 scan lines, and each line is composed of 3240 pixels. The ground size of the pixel determines the maximum resolution of the image. For Landsat MSS images, each pixel represents the average wavelength intensity for a ground area of 79 by 56 meters (Fig. 16-17). Pixel size of Landsat TM images is 30 by 30 meters,

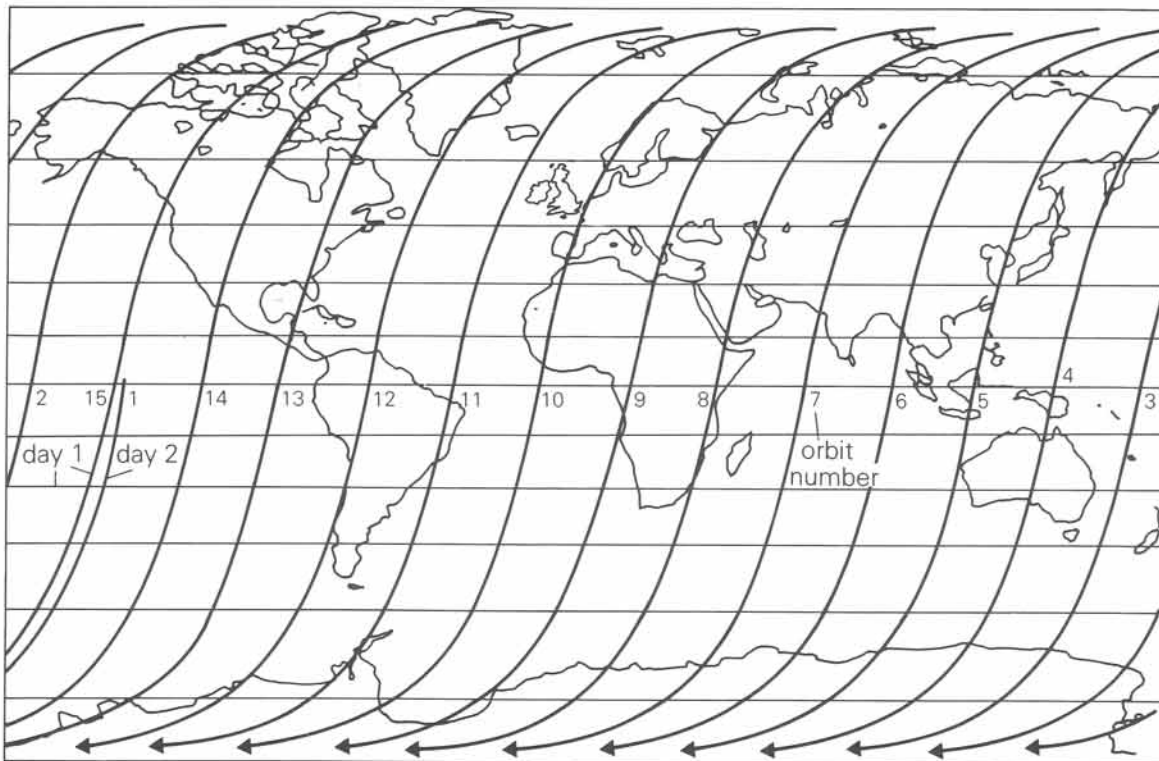


Figure 16-18: Ground tracks of successive Landsat orbits with arbitrary flight path numbers. Orbits descend at day side, shown here, but ascend at night side of the Earth.

while pixel size of SPOT is 12 by 12 meters for panchromatic and 20 by 20 meters for color images.

The area covered by satellite images is commonly limited by the width of the swath covered by the sensor array, either fixed or connected to a scan mirror sweeping back and forth. For Landsat, the standard image covers 185 by 185 kilometers. SPOT, which has a fixed array of electromagnetic sensors and no sweeping mirrors, covers a smaller ground area of 60 by 60 kilometers in each image. Landsat circles the Earth in near-polar orbits once every 103 minutes, between 800 and 900 kilometers altitude, and is sun-synchronous. All images, therefore, receive radiation from the visible electromagnetic spectrum, and nearly the same point on the ground is repeated every 18 days. Each orbital swath is 2,760 kilometers west of the immediate predecessor (Fig. 16-18). The ground-track of the swaths do not closely follow meridians, but are oblique to them, because the Earth rotates away underneath the satellite, which follows a near-polar orbit. Incidentally, the name of the Landsat program was given as a complement to the Seasat program, as it was designed to obtain information from land rather than sea areas. However, Landsat was launched before Seasat and was initially called ERTS.



Figure 16-19a: Part of Landsat MSS of dextral Moroccan Border fault, separating Tindouf basin of the Draa Plateau to the south from tightly folded Devonian limestone and sandstone in the north wall.

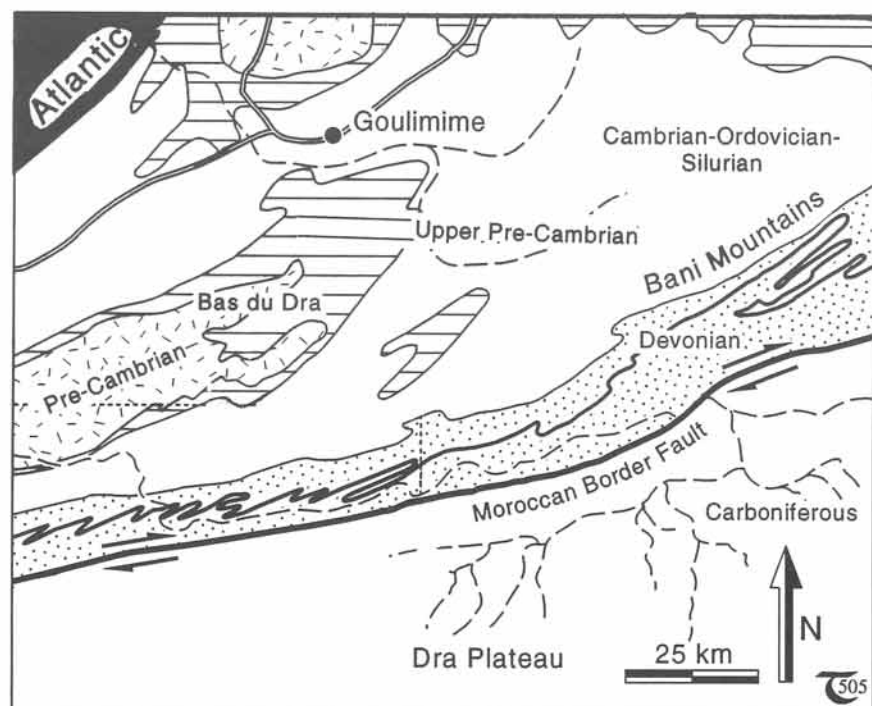


Figure 16-19b: Interpretation map of Landsat image of Figure 16-6a. Precambrian basement inliers are ruled and shaded.

SPOT, an acronym for Satellite Probatoire pour l'Observation de la Terre, is a Swedish-French satellite system, first launched in 1986. Three SPOT satellites concurrently track the ground surface in different polar orbits, completing one revolution every 101 minutes. They are orbiting 830 kilometers above the Earth and complete 14 orbits every 24 hours. Because the Earth turns under the satellite, the ground track of each orbit is 2,823 kilometers farther west of each previous orbit. SPOT images are not composed of line-scans but are measured directly by an array,

consisting of thousands of micro-detectors or charge-coupled devices (CCD's). The radiation from the ground is directly measured without any mirroring, as the CCD-array moves with the spacecraft over the ground area. In multispectral mode, 3,000 CCD's sample the ground pixels, leading to a pixel size of 20 meters. Panchromatic images are built up from 6,000 CCD's and produce a pixel size of up to 12 meters.

The pixel resolution on SPOT images is still one to two orders of magnitude less than that of

low altitude aerial photographs, but better than that of Landsat. Figure 16-19a is part of a composite image of southern Morocco, 150 km from E to W and 225 km from N to S, taken from 817 km altitude by the Landsat spacecraft on March 27, 1973. A geological interpretation is outlined in the map of Figure 16-19b. For comparison, a SPOT image of part of the region is shown in Figure 16-20. This arid region, with only 10 to 15 centimeters of annual precipitation, exposes a geological history from the Precambrian to the present. The semicircular Precambrian basement inlier of Sidi Ifni, near the Atlantic in the northwest (black), is covered by gently folded sedimentary rocks of Paleozoic age. In the south, the meandering Draa Valley

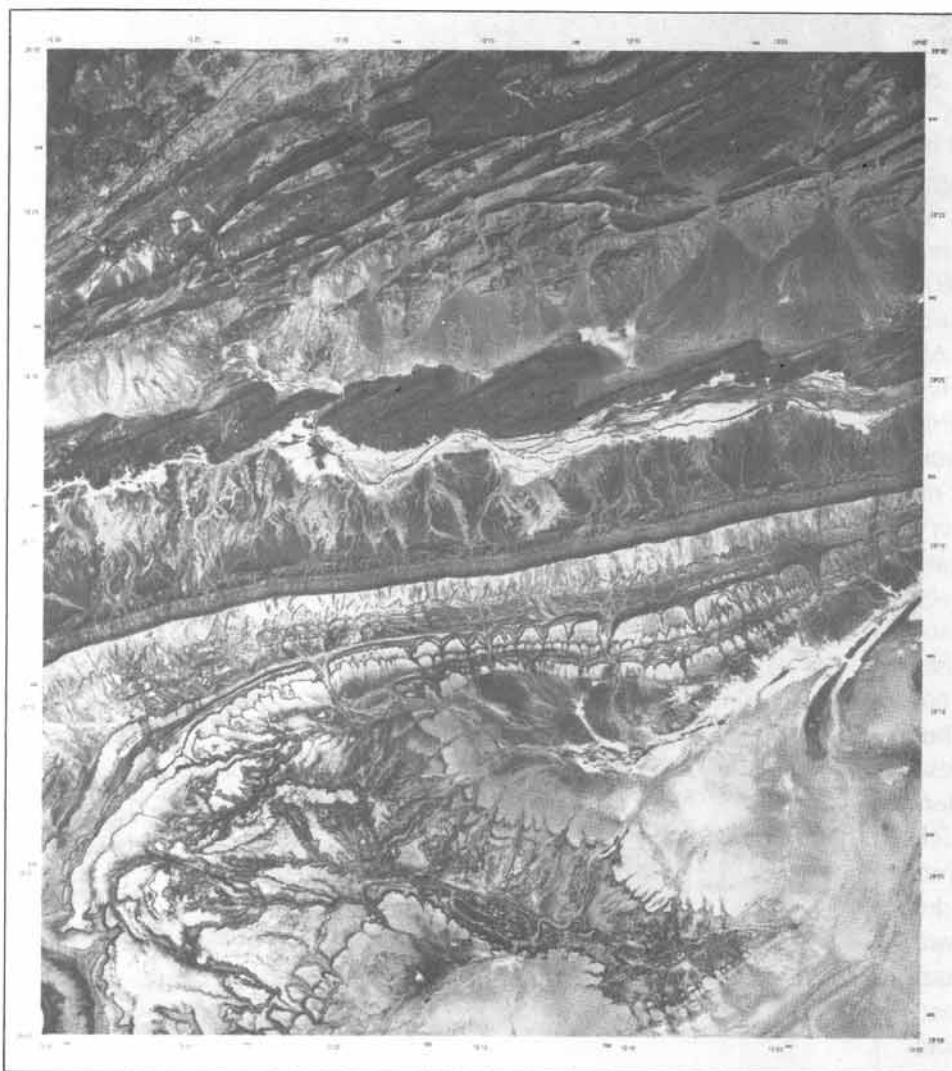


Figure 16-20: SPOT image of Draa Plateau and Draa Valley, immediately south of the folded Devonian sequence. Image width is sixty kilometers. Compare pixel resolution with that of Figure 16-19a.

(white) covers the dextral Moroccan Border fault, which separates the subhorizontal Carboniferous sequence of the Tindouf basin in the south wall from the tightly folded Devonian limestone and sandstone in the north wall. The dextral sense of displacement along the Moroccan Border fault is obvious from asymmetric folds in the Devonian sequence in the north side of the fault.

□ **Exercise 16-7:** Make a geological interpretation map for the area imaged in Figure 16-20. Accompany the map with a written outline, covering, also, the topics discussed in points 1 to 10 of section 16-4.

16-7 Basic image processing

One basic step in image acquisition is the assessment of the original ground data and translating this into pixel tone or color for each pixel. The analogue data from each electromagnetic detector are electronically filtered and calibrated. The quality of the final signal is dependent on the signal-to-noise ratio, which is controlled by: (1) the sensitivity of the detector for recording a particular wavelength, (2) the width of the waveband, (3) the intensity and range of radiation received from the ground surface, and (4) sensor altitude and spacecraft velocity. The scans are beamed down to a ground station in digital form, where they are corrected for distortions.

The actual image is obtained by modulating and rebuilding the scan into an image of pixels, which may be either in color or panchro-

matic (i.e., exclusively in gray tones). This is commonly achieved by scaling the energy of a waveband received by a detector for each pixel with a digital number (DN). Figure 16-21 shows an example of a histogram, showing the frequency or number of pixels that received energy, as expressed by DN's between 0 and 255 for computer compatibility. DN-values of zero correspond to a minimum intensity for electromagnetic radiation wavelengths received (black on the image), and maximum values are scaled as 255 (white on the image). Intermediate brightness values are represented by intermediate DN's and gray shades on the image.

After scaling the basic radiation signal by DN's, image patterns can be described in strictly numerical terms by locating each pixel with an XY position on the image surface, together with a corresponding DN for tone or color value. An example of spatially arranged digital pixel values is illustrated in Figure 16-22a. The energy level of electromagnetic radiation represented by each pixel can be better visualized by assigning particular gray tones to a range of close DN-values. The corresponding computer print-out in gray-scale display is shown in Figure 16-22b. Similar-

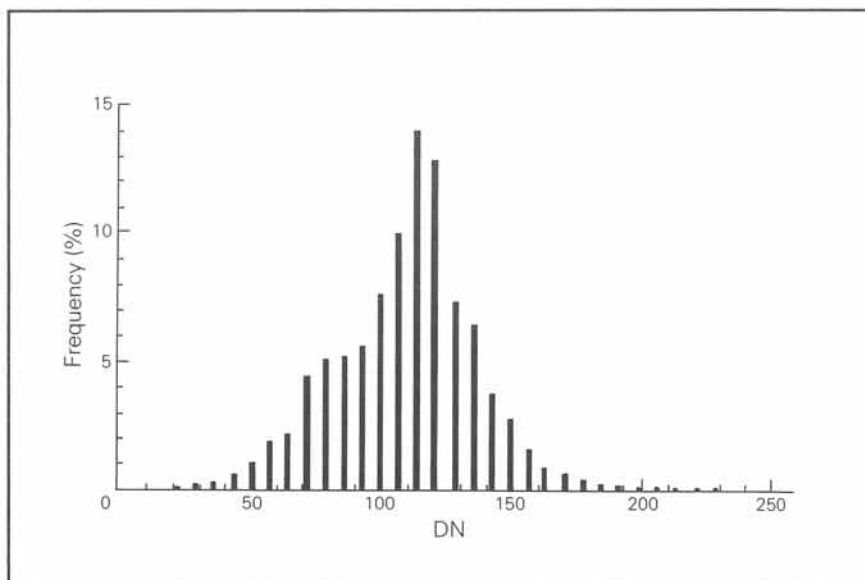


Figure 16-21: Number or frequency of pixels that received electromagnetic energy of the level indicated by a Digital Number (DN), scaled from 0 to 255.

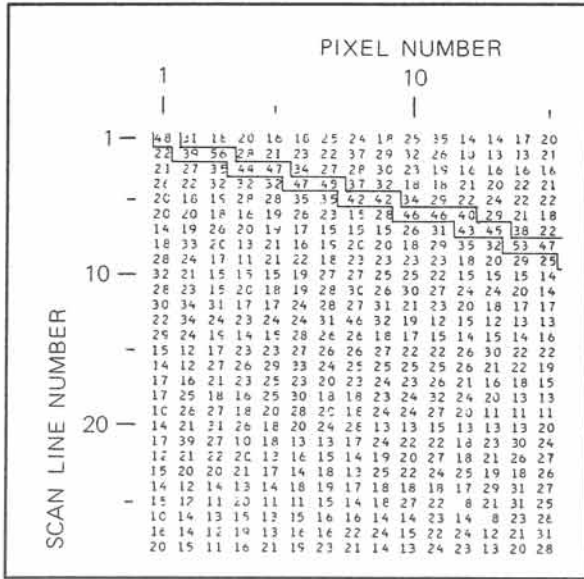


Figure 16-22a: Spatial arrangement of pixels and their DN values in digital image.

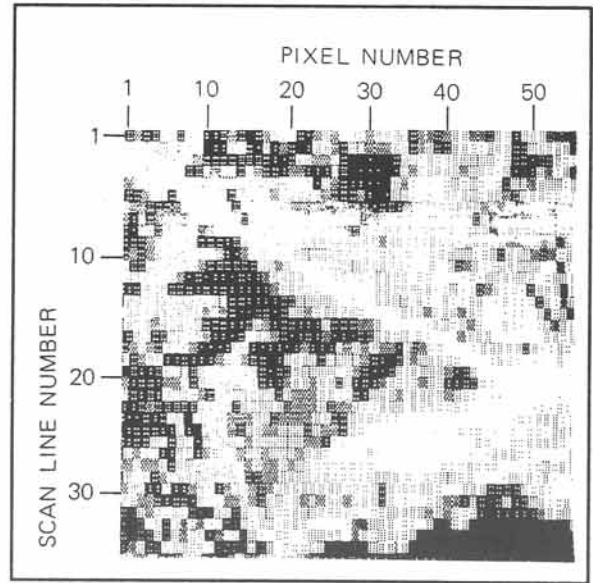


Figure 16-22b: Pixels of digital image, scaled by gray scale display.

ly, a color display could be generated by assigning particular colors, rather than gray tones, to each DN or to a group of DN's. If the colors are different from that of the original colors on the ground such an image is called a false or pseudo color image.

One type of image enhancement can be achieved by manipulating the digital data so that pixels with relatively small differences in DN are displayed with distinct contrast either of color or in gray tones (Fig. 16-23a & b). The density contrast stretching enhancement is principally achieved by reassigning a broader range of DN's to pixels receiving 92 percent of the radiation. In the example shown, an original DN of 49 is rebased to DN of zero, and an original DN of 106 is rescaled to 255. The intermediate values are stretched in between to enhance the contrast in DN's, and the resulting image shows much clearer contrast between ground features of different albedo. Other forms of image processing are aimed at restoring bad sectors due to malfunctioning of the electromagnetic radiation detectors. The image is restored by assigning DN's intermediate to neighboring pixels if original data are missing.

Processing methods can, also, concentrate on the visualization of the energy exclusively received within a particular band of wavelengths. But, if various types of detectors are used in the remote sensing platform, this allows for blending and separation of wavelength bands. The image can be redressed by ratioing bands. For example, the Landsat MSS system can provide each pixel with the energy levels of, at least, four wavelength ranges (Bands 4 for visible green light, 5 for visible red light, and 6 and 7 for parts of the reflective infrared spectrum). Landsat's TM detects seven bands within the electromagnetic spectrum: reflected blue, green, and red light, and four infrared bands. Particular bands favor rock contrast, while some combinations may obscure their distinction. For example, Figure 16-24a shows good bedrock contrast in an area of south India, using Landsat MSS band 7 only. Figure 16-24b displays the same area, using the band 7 and band 5 ratios. This brings out the spectral properties of vegetation but obscures the radiation of underlying bedrock units. Processed images may show rock types in different, false colors, although the original scanner does not necessarily measure any true colors.

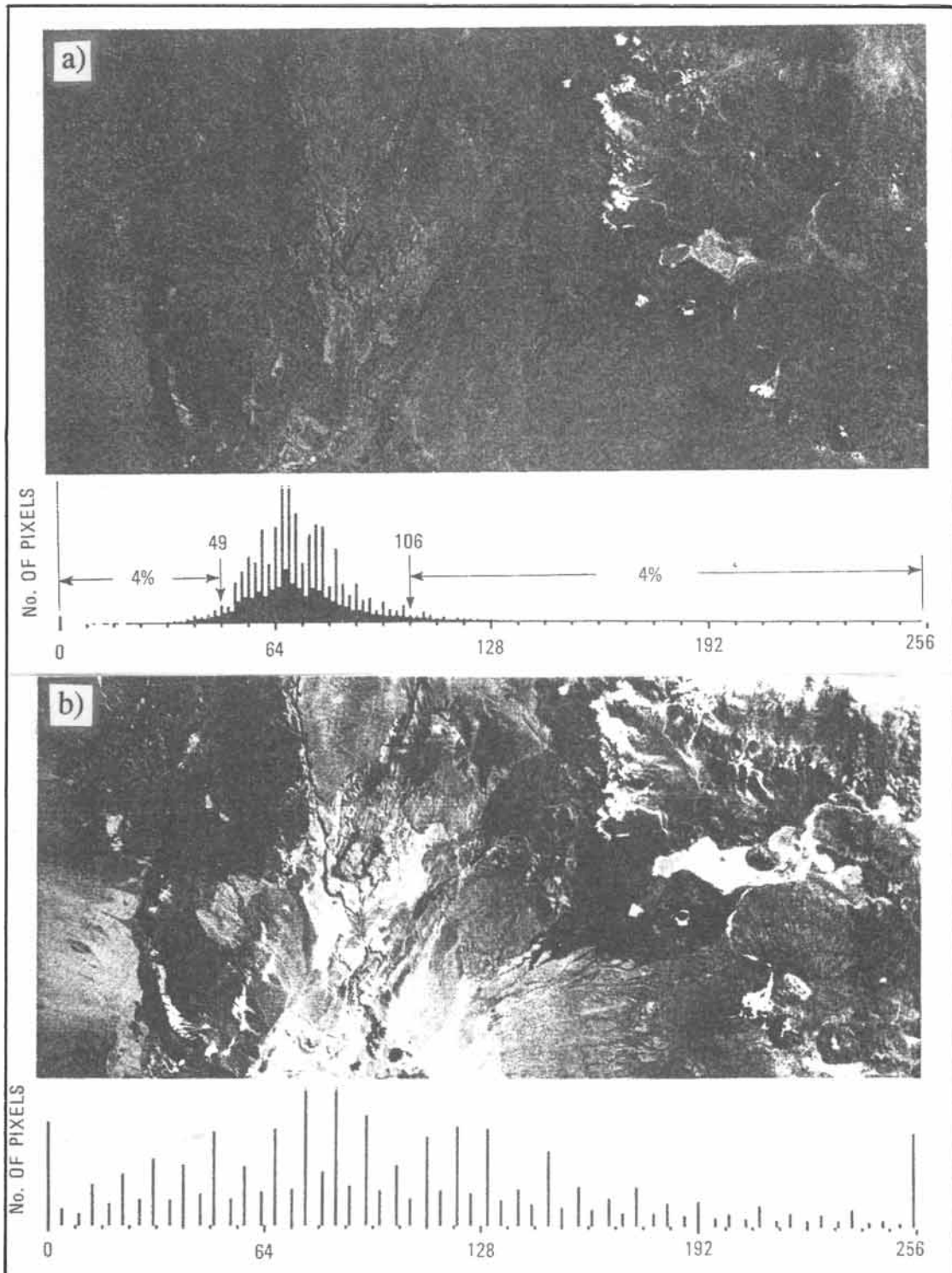


Figure 16-23: a) & b) Image contrast enhancement by stretching. (a) Original image has poor contrast, due to clustering of DN's in histogram of pixel frequency versus DN count. (b) Stretching of DN values of pixels increases contrast in the image.

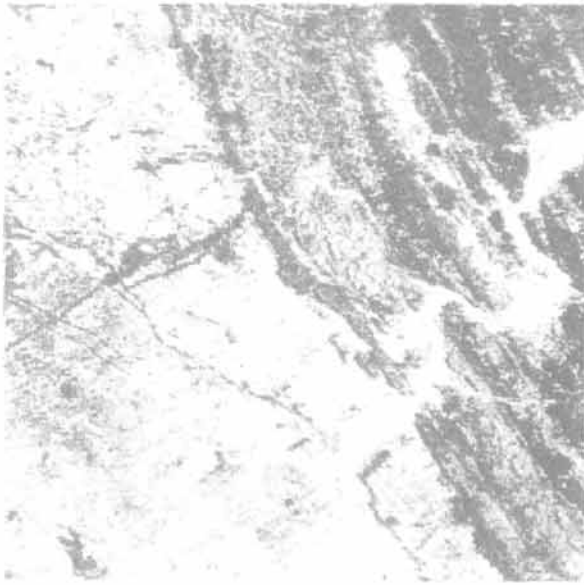


Figure 16-24a: Landsat MSS image, using Band 7 only.



Figure 16-24b: Same Landsat MSS image of Figure 16-24a after ratioing of Bands 5 and 7.

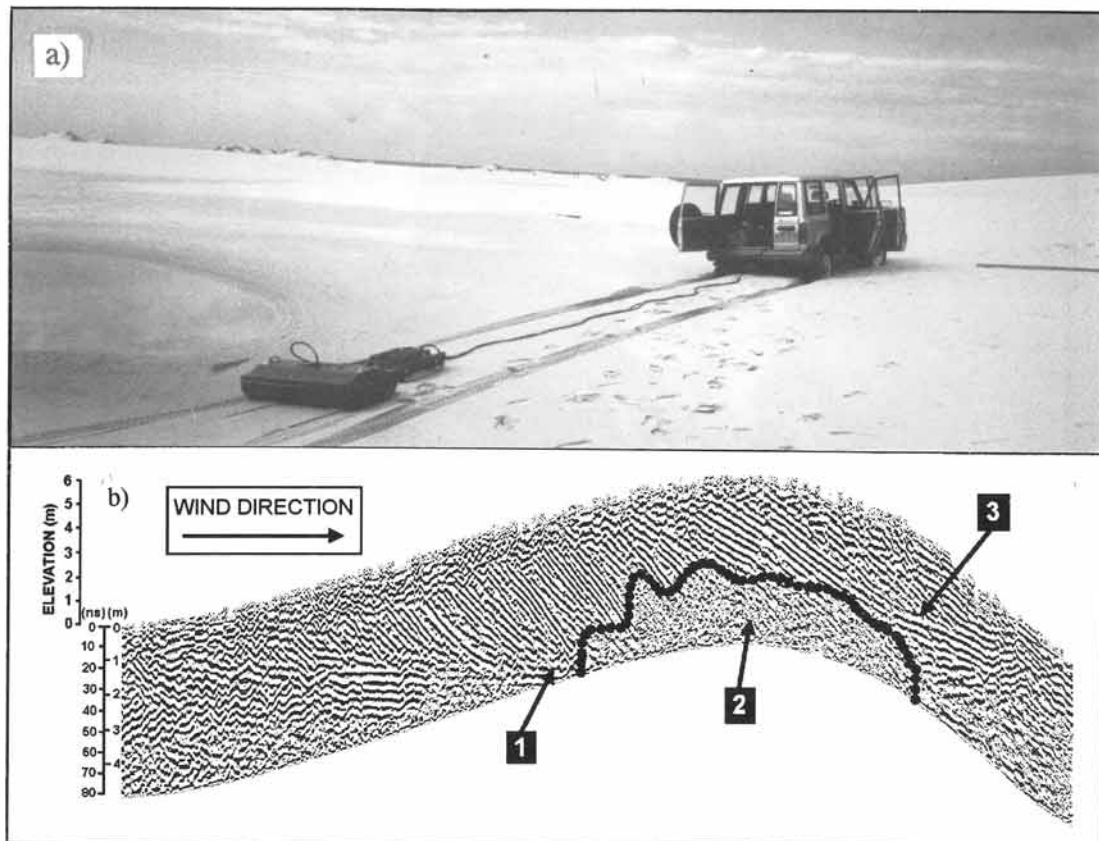


Figure 16-25: a) & b) Ground Penetrating Radar system, towed behind a truck, can produce radargrams that resolve: (1) base of the dune, (2) zone of moisture, and (3) cross-stratification.

□ **Exercise 16-8:** Convert the digital pixel print of Figure 16-22a into a color image by assigning colors to particular DN's.

16-8 Radar images

Radar (radio detection and ranging) has been traditionally used by military and civilian aviation authorities to monitor air space and ships at sea. It detects microwaves, which easily penetrate clouds, is insensitive to meteorological

conditions, and is independent of daylight. The letter-coding of K, X, and L-bands (Fig. 16-1) originates from the Second World War, when it was used for security reasons.

In modern radar-imaging systems, microwave pulses generated by an antenna, are directed towards the ground surface. Radar wavefronts are backscattered and received by the same antenna before another pulse is emitted to the ground. The system can be carried in an aircraft, boat, or spacecraft. Ground Penetrating Radar (GPR) is a ground-based, remote sensing tool, used for non-destructive subsurface inves-

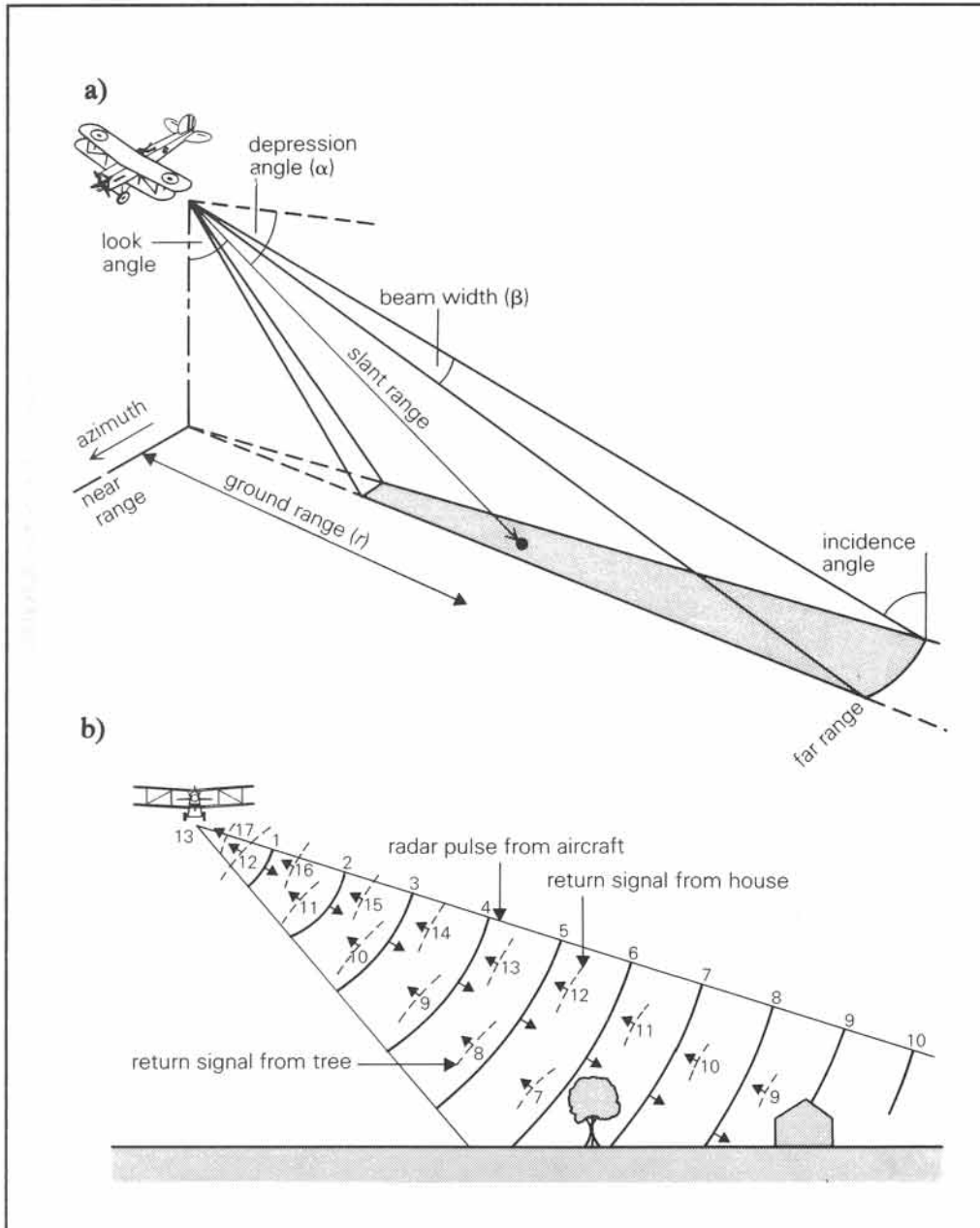


Figure 16-26: a) & b) Airborne radar is "side-looking" and distortions in the slant range increase with the incident angle of the pulsating radar signal.

tigations. The antenna array is towed behind a truck and data are recorded in the field on a magnetic tape (Fig. 16-25a). The system differs from airborne radar in that the wave form is recorded in addition to the intensity. After processing the data in the office on a work station, the resulting image resembles a shallow seismic section, showing horizontal distance versus two-way travel time in vertical cross-sections (Fig. 16-25b). GPR can be used for mapping shallow geological structures down to twenty meters deep in dry sand.

Air and space-borne radar images typically have a sidelit character, resulting from cross-scanning of the surface while being overflown (Fig. 16-26a & b). Radar pulses can be transmitted in different modes of polarization, with vibrations restricted to a particular plane parallel to the direction of radar emission. Airborne radar images commonly have a fifty-kilometer-wide swath and resolution cells or pixels of ten to twelve meters width. Most commercial radar uses the K and X bands, which have negligible ground penetration. The backscattered electromagnetic



Figure 16-27a: L-Band radar image, collected by Space Shuttle Endeavour from Wadi Sahba area, Saudi Arabia. The trace of the E-W trending Sahba fault is clearly visible. Image width is 40 kilometers.



Figure 16-27b: Landsat MSS image across same area portrayed in Figure 16-27a shows bedrock structures are entirely obscured by Ad Dhana sand sea. Thin E-W line in image is railway track.

energy is controlled by the roughness and heterogeneity of the surface materials, their electrical properties (expressed in a dielectric constant), the slope of the ground surface, and the nature of the original microwave signal used to illuminate the ground surface.

Radar images have, also, been collected by NASA space shuttles carrying sophisticated radar systems. These include the L band, which may penetrate to six meters in depth into dry sand deposits. Moisture absorbs radarwaves, because the dielectric constant is greatly affected by the

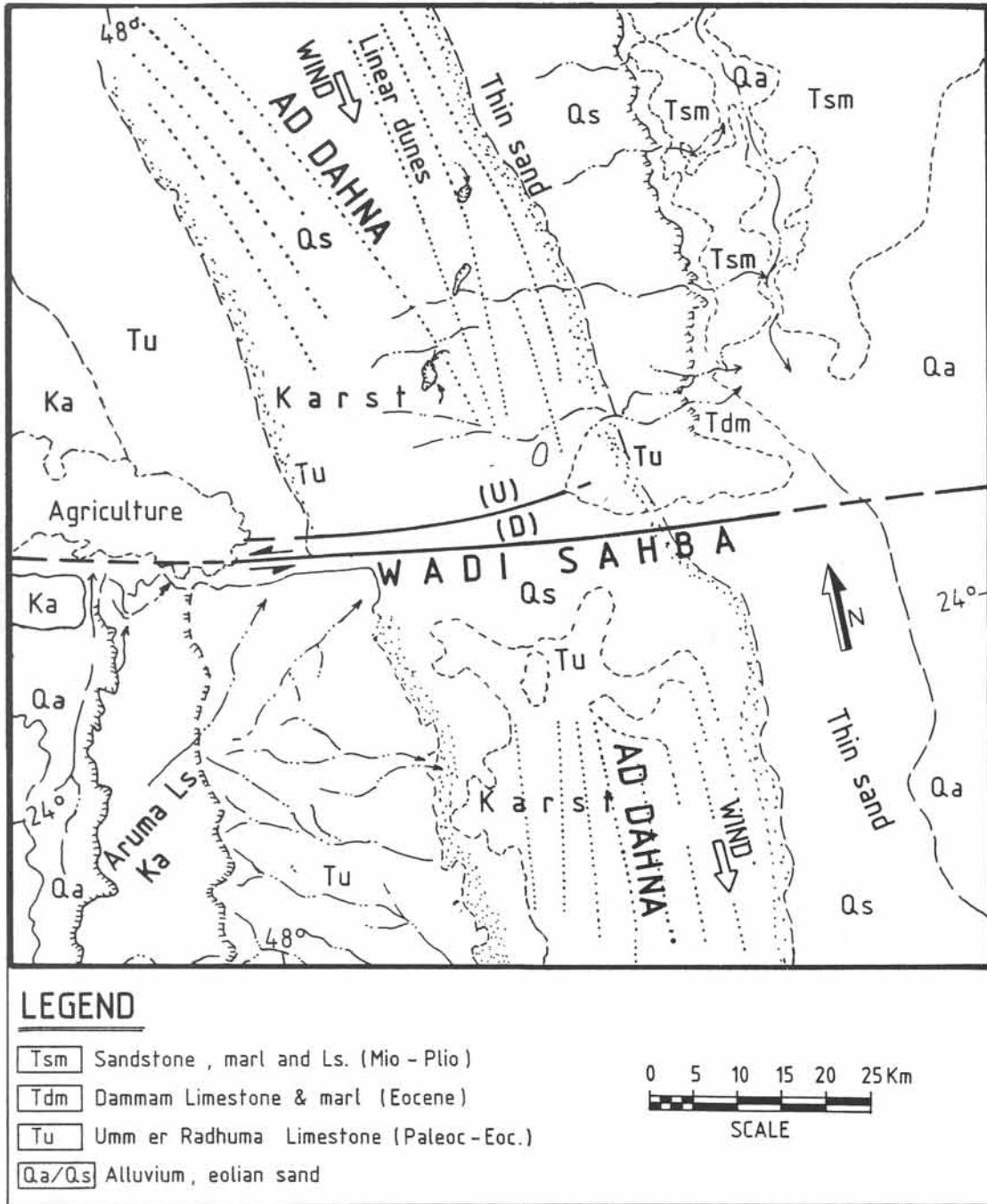


Figure 16-28: Geologic interpretation map of the Sahba fault, Saudi Arabia.

moisture content of the ground and, thus, reduces the penetration depth of radar methods.

Radar images using the L band may reveal shallow subsurface features, invisible on other remote sensing images. For example, the radar image of Figure 16-27a stretches across a section of Wadi Sahba, Saudi Arabia, where lower Tertiary strata are largely covered by the Ad Dhana sand sea. The drainage pattern and karst terrain incised in the bed rock below the Quaternary dune sand are clearly visible in the area north of Wadi

Sahba, where the thickness of the sand sheet varies between two and ten meters. Such drainage patterns are relatively absent to the south along Wadi Sahba, where sand thickness exceeds ten meters and radar microwaves cannot reach the bedrock. The apparent change in bedrock depth on either side reflects a vertical component of relative movement. Topographic relief along the fault has been leveled by the drifting sand, which infills the low area on the south side of the fault. The Landsat image of Figure 16-27b confirms that the fault line is hidden beneath the eolian

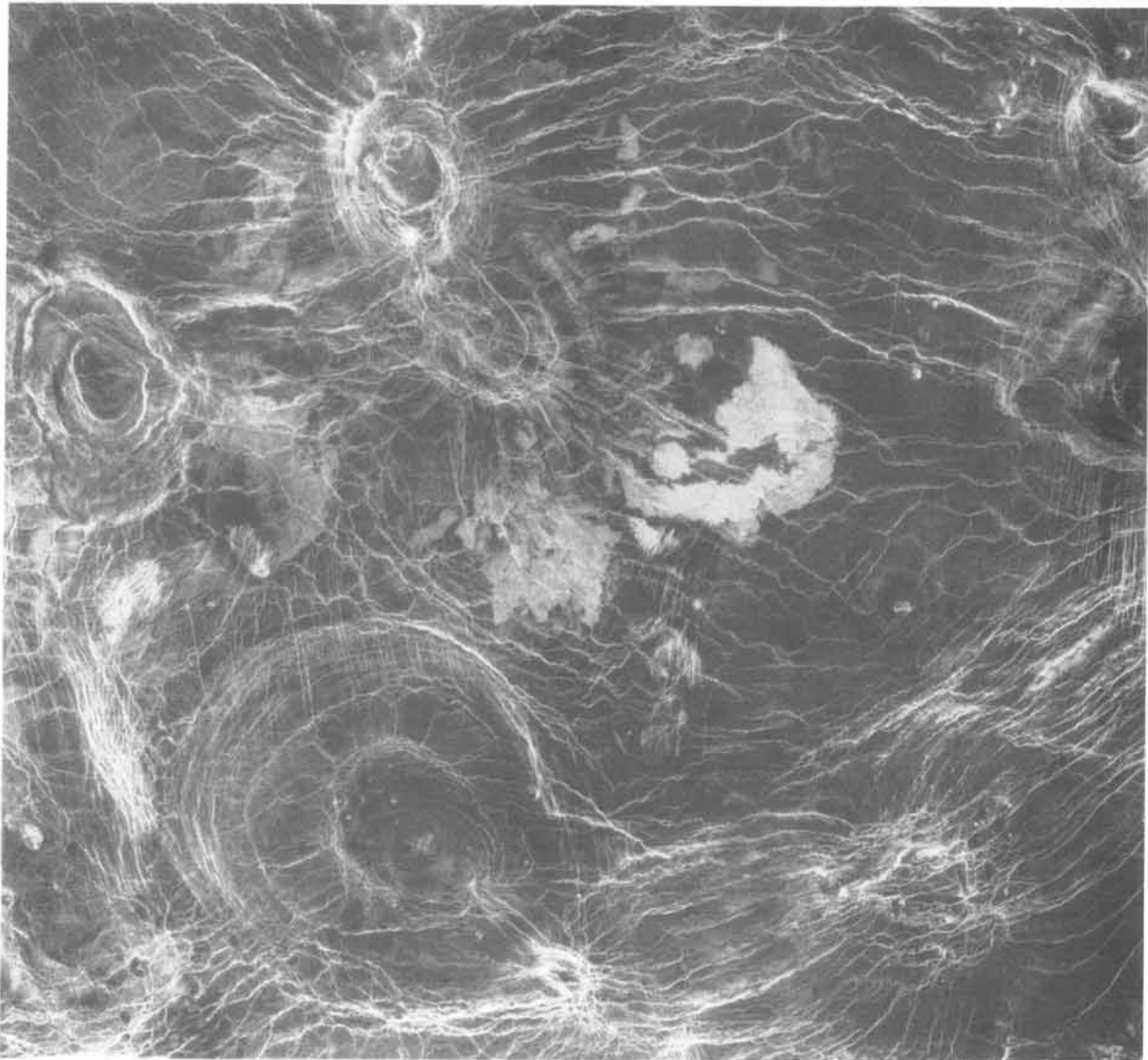


Figure 16-29: Radar image collected by NASA's Magellan space probe from the surface of Venus. Shown are arachnoids with diameters ranging from 50 to 230 kilometers.

sand and is revealed only by radar penetration along its northern side. The image interpretation map of Figure 16-28 indicates eight kilometers of apparent left-lateral displacement at the western end of the Wadi Sahba fault. This off-set is marked by exposed bedrock of Paleogene limestone.

Radar imaging has, also, been successfully used to explore the surface of various neighboring planets using a range of spacecraft missions. For example, Magellan is a NASA spacecraft launched in 1989 from aboard the Space Shuttle Atlantis. The spacecraft began its orbit around Venus in August 1990. A synthetic aperture radar (SAR) was used to penetrate the thick cloud cover, perpetually shielding the surface of Venus from vision. Figure 16-29 shows features, known as arachnoids, that have thus far been found on

Exercise 16-9: Color the map of Figure 16-28 and compare this interpretation map with the original image of Figure 16-27a.

Venus only. They resemble spider and cobwebs and are circular to elliptical in shape with concentric rings and intricate outward-extending fractures. Arachnoids have diameters ranging from 50 to 230 kilometers. The bright lines, extending outward for many kilometers, may be dikes formed when magma upwelling from the planet's interior caused surface cracks. Arachnoids could be subvolcanic complexes with annular ring dikes and cone sheets, and radial igneous dikes. The bright patches in the center of the image are lava flows, indicating volcanic activity.

Chapter 17: Computerization of Map Analysis

COMPUTER LITERACY certainly is helpful in any modern profession, and this applies particularly to the earth sciences. Visual images - including geological maps and cross-sections - are an important part of our profession. The display and manipulation of geological graphics can be greatly facilitated by digital image processing. Limited computer capacity and excessive cost have previously constrained wide-scale application of digital image processing. But, technological innovations are continually optimizing computing capacity. Professional systems, although still expensive, are becoming more affordable and, consequently, are more widely available. Not surprisingly, software programs for geological applications are rapidly improving and diversifying. These applications include map display, sectioning operations, and reservoir modeling. This chapter discusses some of the options currently available. Additional resources, including geological software and data processing services, are listed on page 367 and onward.

Contents: The digital future of map representations is discussed in section 17-1. Hardware and software items are summarized in sections 17-2 and 17-3. Geographical Information Systems are introduced in section 17-4. The promising development of dynamic digital maps is highlighted in section 17-5. Some hints for on-line resources of maps are given in section 17-6. The role of interfacing platforms in industrial applications is explained in section 17-7.

17-1 Digital geoscience

A clever practitioner of map interpretation will use any technique which adds to the quality and validity of the result. The role of computerized map analysis can be important in this process. Computer applications are coming of age, and

full-fledged automated data manipulation is particularly advanced in geological applications since it involves huge amounts of old and newly acquired field data. In modern geological surveys, nation-wide geological observations are increasingly being stored digitally and mapped using computer databases. Similarly, mining and

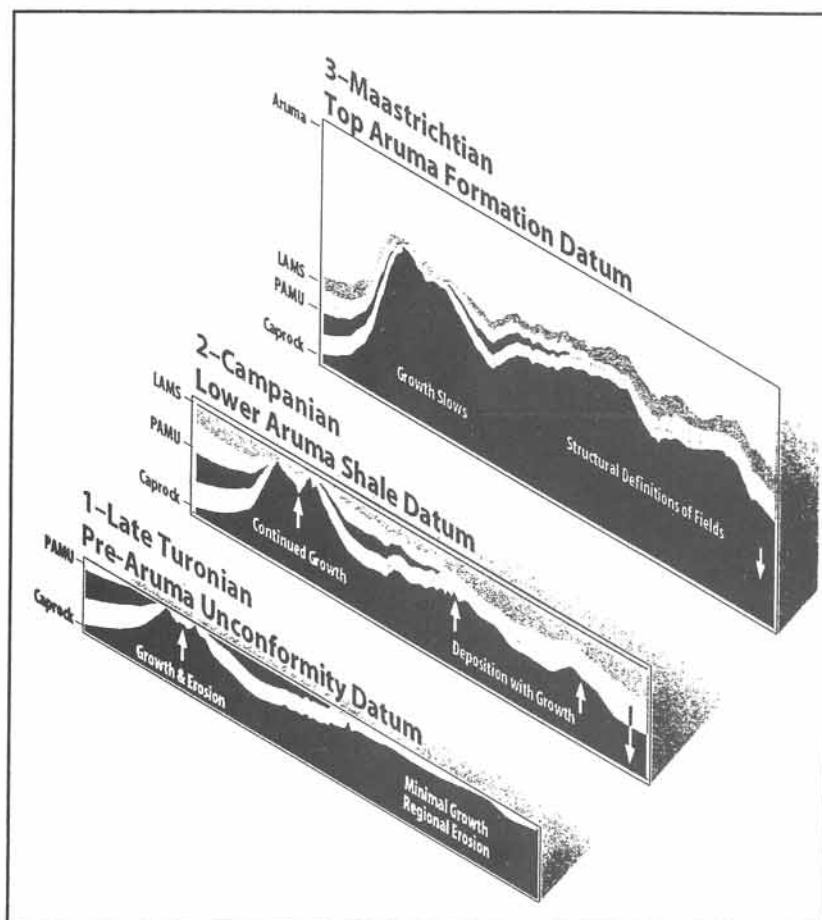


Figure 17-1: Growth history of oilfield below caprock, depicted in cross-sections at three stages of development, Arabian Gulf region.

oil companies are faced with the task of storing and managing enormous sets of data related to prospect areas. These operations are becoming dependent on advanced application programs, which allow the full integration of directly accessible digital data sets.

For example, well-log data are presently recorded digitally at the well-head and can be displayed together with seismic sections and maps, using powerful software packages. These data are part of bigger, compatible databases that are continually expanding and improving. Three-dimensional recording of seismic data enables the graphic display of subsurface structures from any angle of view. All these operations help to optimize well locationing, reservoir management, and

strategic planning. The information processed by current workstations typically are of the order of five hundred Megabytes or more. Team efforts can be compiled on so-called video-walls, which allow the comparison of a dozen images, each routed there from its own workstation. This allows the development of integrated geological models, using 3-D seismic information and structural and stratigraphic data. Reservoir management and mining can be optimized, using this new approach (Fig. 17-1).

Digital image processing not only requires a good grasp of the basic techniques of map interpretation, but also an understanding of the hardware and software that can help to complete the task more effectively. Newly developed software is sometimes clumsy and difficult to use. This can be a nuisance to users who are preoccupied with a multitude of other tasks. Computer programs, if not used on a regular or routine basis, consume considerable time

to reacquaint the infrequent user. Most geologists, concentrating on the actual mapping of rock units and the associated structures in the field, have too little time to maintain a skill-level required for digital image processing of complex geological maps. Such data manipulation is best done in a team operation, where experts can combine their different knowledge and skills to achieve professional results. This still means that geologists need to understand, at least, some basic principles of digital map systems in order to communicate effectively with the operator of such systems. However, the operator, performing the map analysis, may well be a weathered geologist, who has later concentrated on data-processing and computer skills.

The preceding chapters were aimed at developing a thorough grasp of the basic principles of map interpretation. This was achieved by practicing manual exercises of analog construction techniques. However, the future of map interpretation is in digital image processing, and geologists need to understand, at least, the basic principles of the available technology. One way to achieve this is to increase your computer literacy at every opportunity.

17-2 Hardware

Advanced digital image processing involves considerable investment in hardware (the machine) and software (the interactive instruction program). Detailed knowledge of the technical capacity of hardware is essential for a smooth and professional performance. The hardware required for digital map analysis involves the computer, its monitor, and accessories. Before making any choices, it is essential to check carefully which software is compatible with your computer system. The kind of hardware accessible to you determines your possibilities. Digital image processing involves a large number of data or bits, so that a reasonable processing speed is required. The development of the technical standards in this area is much faster than the time required for this book to be printed. It is, therefore, beyond the scope of this book to survey the available hardware in any depth, and only some guidelines are provided here. This section concentrates on PC platforms for instruction purposes. However, to perform the mapping, cross-sectioning and other modeling functions, most oil companies now use local networks with SUN or SGI UNIX workstations connected to mainframe computers (e.g., IBM, Cray, Amdahl, DEC, or Hewlett Packard).

The processing speed of your computer is to a large degree dependent on the type of microprocessor (or microchip) used to build the central processing unit inside the computer. Use modern software on a modern computer. The main memory, residing in a section of the central processor unit, includes both a ROM-unit (read only memory) and a RAM-unit (random access memory).

Additional mass storage memory is provided by various types of resident memory (hard disk) and by removable disks. Sufficient RAM-capacity is particularly important. Some user programs cannot be implemented on computers with a small RAM-size. For example, *AutoCAD* - a powerful graphics utility program with many geological applications - presently requires a minimum of four megabytes RAM. It, also, requires your machine to include a rather costly math coprocessor - a booster for the central processing unit - to enable rapid data manipulation. The latest microchips have math coprocessors built in.

The chip-speed is not the only factor controlling the processing speed, because the amount and speed of the main memory and caches, also, play a role. Nonetheless, Intel's microchips are most widely used, and the present generation is characterized by the 5xx-series (including the Pentium Pro), which supersedes the xx486-digit series. Older generations of microprocessor units bear labels coded 80386, 80286, 8086, 8088, 8085, 6800, 6502, and Z80. New generations of chips are likely to enter the market by the time this book reaches you. In order to allow your computer to display graphics, you may need to purchase an optional graphics card for the vacant slots inside your machine. A high resolution (minimum 640 by 480 pixels, VGA) color monitor with a large format screen is, also, desirable for any kind of professional image processing. Sophisticated image manipulation further requires special equipment to transfer the image from the monitor to a hardcopy medium. This may include large format color printers and inkjet plotters, the quality of which is rapidly improving.

You, also, need accessories that allow the feeding of raw data into the machine. Map data can be drawn entirely from scratch onto the computer screen, but this is uncommon. Digital maps may be based on topographic maps, existing geological maps, aerial photographs, or satellite images. Base maps need to be fed digitally into the computer. There are several ways to achieve this: a) Reading of existing digital base maps, commercially available on CD-ROM. b) Accessing

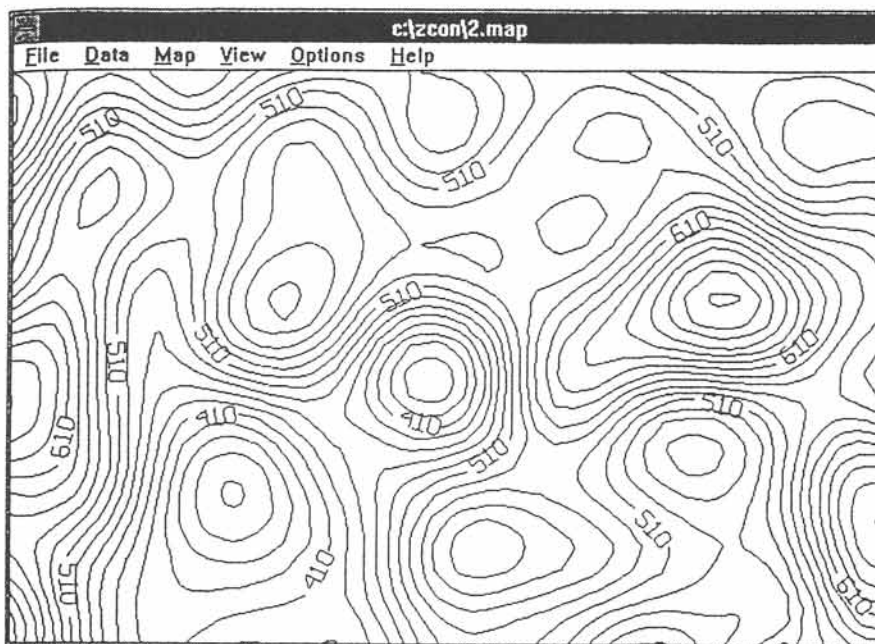


Figure 17-2: Contour map, generated by Z/CON from spaced elevation points.

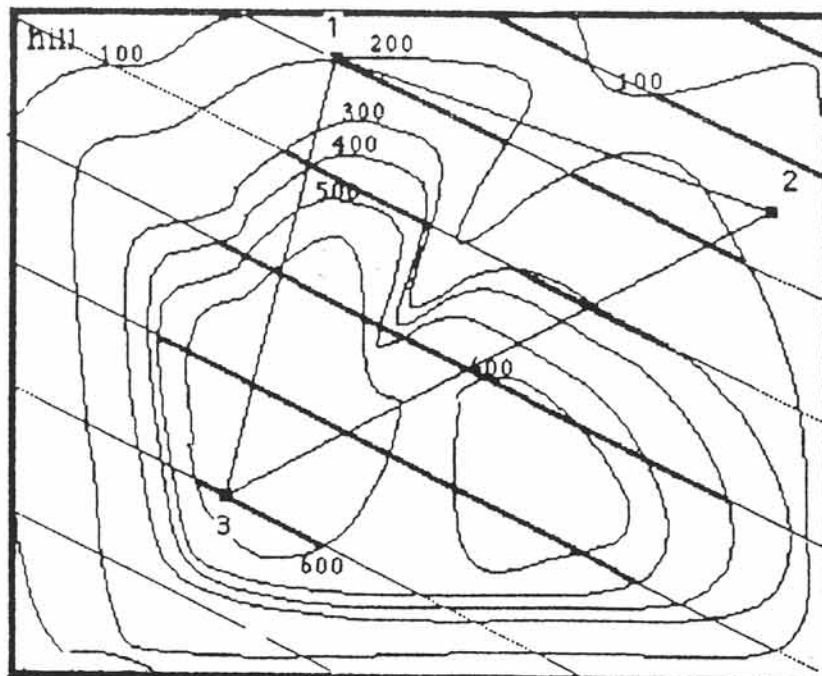


Figure 17-3: Structure contours, drawn interactively by SL-Macintosh on a topographic base map, generated by CNTR.

existing digital map files via Internet (see section 17-6). c) Digitizing your own hardcopy maps with the help of a digitizing tablet and supporting software to create the data file. d) Scanning your own hardcopy map with the help of a scanner unit and supporting software to create the data file. The methods referred to above require the following hardware: (a) CD-ROM drive, (b) Internet modem, (c) digitizing tablet, and (d) scanning unit. This equipment must be connected to, and correctly communicate or interface with, your computer. Special software is required for creating the digitized or scanned data files (see below).

One thing that seems certain is that it is hard to keep abreast of advances in hardware development. Larger companies, government agencies, and academic institutions all have special staff to assist you in this task. Smaller institutions have little or no support and typically tend to outsource technological expertise and to lease rather than buy their computer equipment. Ultimately, you may find yourself developing into a computer nerd, by pure necessity.

17-3 Elementary software

When you actually want to try a digital map analysis, the communication between you and the machine is maintained by an interactive user program. The initial choice of software to be

used is a very important one, because data presentations in one program often cannot be readily transferred to or read by another program. Presently, software packages are divided into several groups, based on operating systems: i.e., DOS, UNIX, Windows, or Macintosh. Some very useful programs may be available only for one of the operating systems. Another limitation on your application may result from the processor speed and the various types of memory in your computer.

In order to get started with digital map analysis select a program that performs the particular type of geological map analysis required and then make it work on your computer system. The type of software you need depends on what you want the computer to do for you. There are simple and inexpensive software packages for small tasks, such as producing contour maps from elevation data, or a single type of block diagram. More sophisticated (and costly) packages have many subprograms, which allow contouring, cross-sectioning, and perspective drawing for arbitrary angles of view. This section concentrates on software for use on PC's and Macintosh computers. For comparison, some main UNIX software company offerings include *Zmap*, *Stratamodel* and *Stratworks* by *Landmark*, and *CPS-3* and *Stratlog-2* by *Schlumberger*.

Although some examples of commercially available software are outlined below, much more is available from a variety of sources. No attempt has been made to assess the quality of any products. Prospective users are advised to critically evaluate the performance and functionality of individual products. Suppliers of geological software and services are included in the final section, *Additional Resources* (p. 367 and onward),

DIGITIZE-Macintosh & PC: This is a digitizing program, which creates an ASCII data file from analog drawings. You need an electronic digitizing tablet plugged into a serial port of your computer. An electronic pointer is used to trace the analog coordinates of the graphical elements from a map taped to the digitizing tablet. The



Figure 17-4: Perspective landscape of Mount St. Helens, processed from elevation-data files (DEM), using GRIDZO.

data files thus created can be read with more advanced software for further manipulation and display of the digital drawings. Digitizing tablets are supplied by a range of manufacturers but not that not all digitizing software runs on all tablets. Check what software is suitable for your brand of tablet. Details on *DIGITIZE* can be obtained from *RockWare*.

Z/CON-PC: This is a contouring program to generate smoothed and labeled contour maps from ASCII-files with the raw data points (Fig. 17-2). This program is compatible with IBM-PC's equipped with the Windows-interface. Details on *Z/CON* can be obtained from *RockWare*.

CNTR and SL-Macintosh: Contour filemaker (*CNTR*) can be used to digitize points from simple maps after scanning them into your PC. Points on each contour are captured by clicking the mouse to create a digital file of your contour map for further processing. *Structure Lab (SL)* reads the *CNTR*-file and solves three-point and structure contour problems (Fig. 17-3). Sample

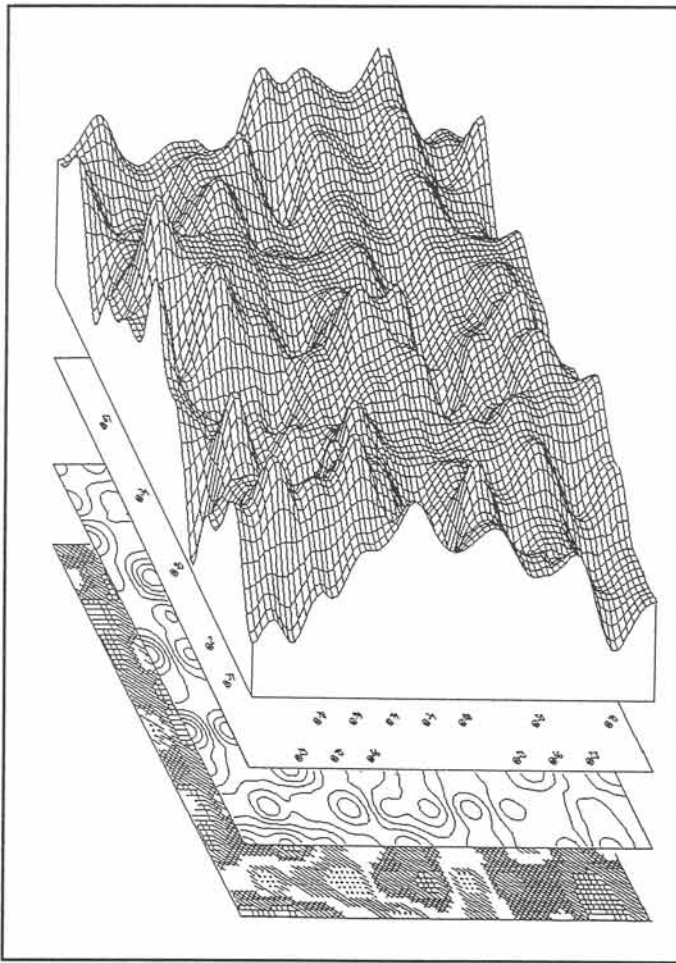


Figure 17-5: Contour maps and fishnet block diagram, drawn by GRIDZO.

maps and a manual for student exercises are included. Details on *CNTR* and *SL* can be obtained from *Earth'n Ware*.

DEM-Macintosh & PC: Digital elevation models (*DEM*) are elevation data files from the *United States National Geophysical Data Center's* data base, compiled from satellite surveys. Each *DEM* covers a 7.5 by 7.5 minute block of any part of the United States. These data files can be read with more advanced software for further manipulation and display, e.g., *GRIDZO* or *3D* discussed below (Fig. 17-4). Details on *DEM* can be obtained from *RockWare*.

3D-PC: This software is designed to transform *DEM*-files into isometric block diagrams of the surface topography. The surface shape can be visualized by colored and raised relief contours or as a shaded relief for different light sources. The block diagram can be viewed from any angle and from different heights above the horizon (Fig. 17-4). Details on *3D* can be obtained from *RockWare*.

GRIDZO-Macintosh & PC: This is a mapping package for producing contour maps and block diagrams with raised contours or fishnet mesh grids (Fig. 17-5). The package includes comprehensive manuals and tutorials. Details on *GRIDZO* can be obtained from *RockWare*.

VistaPro-PC: This is a state-of-the-art landscape simulator, which uses real-world-data from the *United States Geological Survey* and *NASA* to draw relief scenes. Landscapes included are Mount St. Helens of Washington, Crater Lake of Oregon, Olympus Mons of Mars, and El Capitan of Yosemite National Park, California. Synthetic landscapes can be generated with the built-in fractal expressions. Colors and physiographic features, such as trees, snow, lakes, and rivers, can, also, be

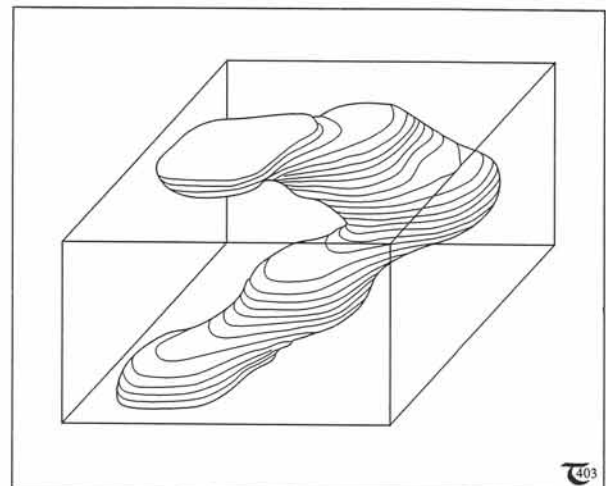


Figure 17-6: Elevated structure contours, outlining the shape of an ore body, drawn by *Rock-solid*.

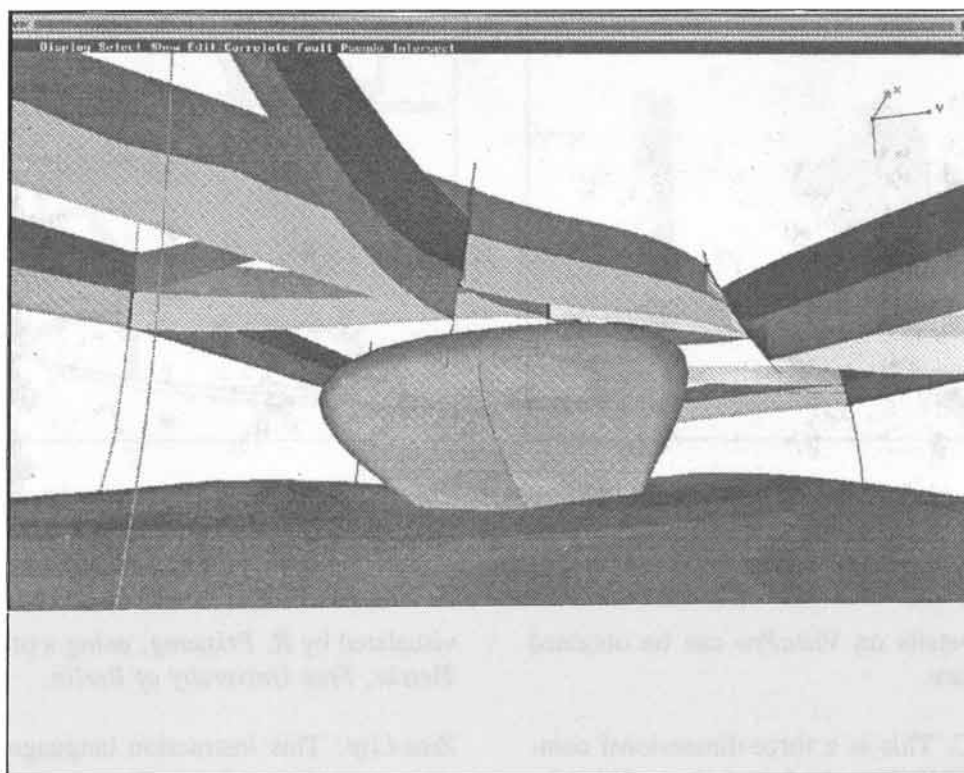


Figure 17-7: Perspective view of salt dome and fence diagram of surrounding beds faulted by the buoyant salt, generated with IREX.

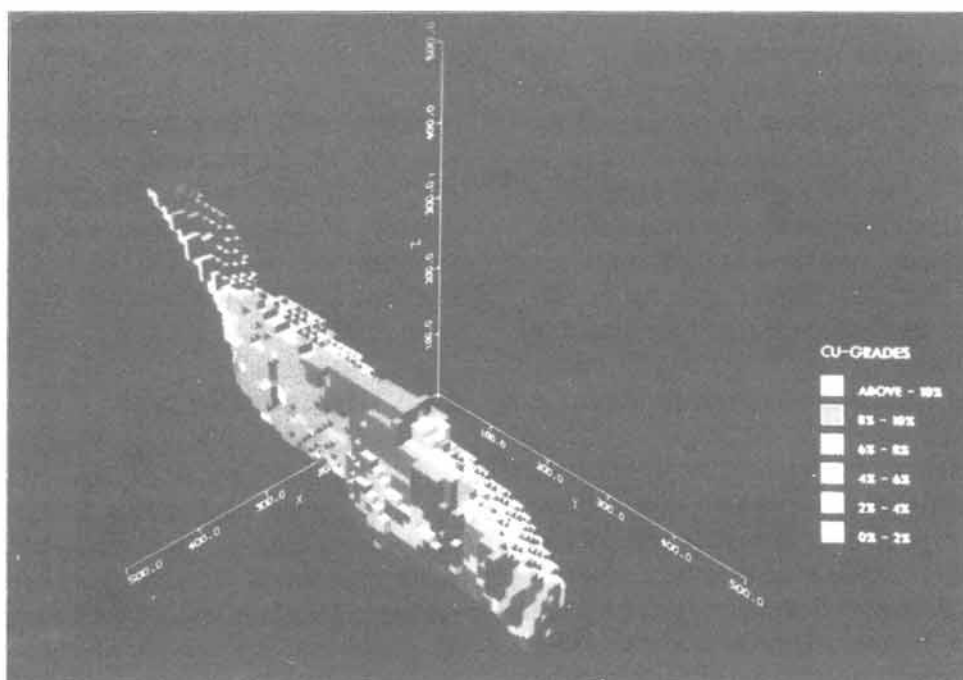


Figure 17-8: Shape and copper-grade of the Cayeli ore body, Turkey, drawn with Ca-Disspla.

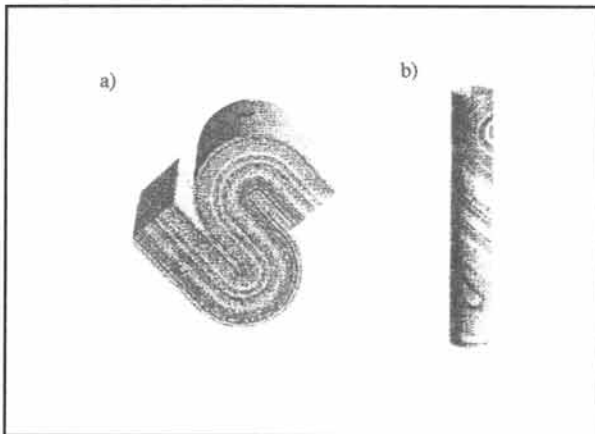


Figure 17-9: a) & b) Overturned isoclinal parallel fold and its appearance in a vertical drill core in perspective views, simulated by *Zeta-Lisp*.

simulated. Details on *VistaPro* can be obtained from *RockWare*.

Rocksolid-PC: This is a three-dimensional complement to *GRIDZO*, which includes utilities for structure-contouring of 3-D orebodies (Fig. 17-6). Details on *Rocksolid* can be obtained from *RockWare*.

IREX: This advanced software package, developed by an industry consortium, runs on Silicon Graphics series of computers. It is designed for high-performance 3-D graphics of reservoir models. Figure 17-7 is an *IREX*-generated perspective view of a salt dome, surrounded by fence sections of the sedimentary host rocks. The faults are marked, and the 3-D display can be swiftly modified when additional data become available from new seismic survey lines and drill cores. Details on *IREX* are available from *TechLogic*.

Ca-Disspla: This is a powerful graphics library, which can be utilized to write your own customized graphics program. For example, object rendering utilities can be used to write a program that enables a display of both the shape and grade of ore bodies in the subsurface. Figure 17-8 illustrates the spatial distribution of Cu-grades by color coded cubes for the Cayeli Cu-Zn-Pb deposit, eastern Turkey. This application was

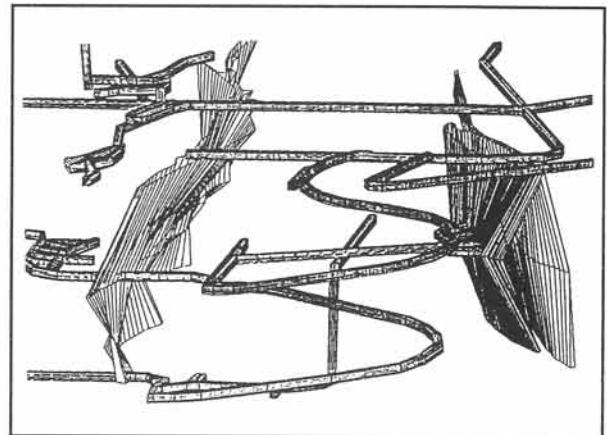


Figure 17-10: Tunnel system and position of steep fault surfaces, generated by *AutoMiner*.

visualized by *R. Prissang*, using a program by *J. Tietske*, *Free University of Berlin*.

Zeta-Lisp: This instruction language, like many others, can be used to write geometric modeling programs. The appearance of deformed layers on the surface of cylindrical drillcores (Fig. 17-9) has been modeled by *Stefan Luthi*, using a graphics program, written by *Kurt Fleischer and Andy Whitkin* of *Schlumberger Research*.

AutoMiner-PC: This software provides a subroutine for, or enhancement of, *AutoCAD*. It is particularly useful for mining applications and the planning of ramps and tunnels (Fig. 17-10). Ore volumes and weight can be calculated from sections. Details on *AutoMiner* can be obtained from *RockWare*.

17-4 Digital GIS maps

Geographic information systems (GIS) form the basis for many applications in modern digital mapping, including geoscience functions. The basic idea behind GIS-databases is to store data related to locations on the surface and subsurface as geographic entities. A number of different databases can be superimposed in data planes and a selection of the relevant data can be combined in a customized map. Examples of data sets suit-

able for manipulation in GIS are electro-magnetic radiation patterns, such as seen in Landsat or Spot images, gravity anomalies, aeromagnetic field strength, terrain models, well locations, infrastructure, geophysical survey lines, spatial variations in geochemical data, etc. Each GIS is adapted for integrating many different kinds of geoscientific data in what is sometimes termed a synergistic analysis. The final database contains a variety of information, all referenced to a common geographic datum.

Before the arrival of computer-based GIS analyses, geologists had to compare maps of a variety of scales, flipping them back and forth while forming a mental model of the integrated data. Interpreting such data becomes much more effective if all the information systems are combined in a geographically-referenced system. Most GIS software packages can import a range of formats from data sets that are obtained in digital format from a variety of sources. For example, digital elevation data are available through some government agencies in North America. Such files include DEM's (digital elevation models), DTM's (digital terrain models) of the USGS, and TIGER's (topologically integrated geographic encoding and referencing), which contain infrastructure data from the US Census Bureau. Other examples are satellite images of Landsat's thematic mapper and seismic epicenter locations which are recorded in digital format from the outset.

The incorporation of geological and geophysical information into digital GIS format was greatly simplified by the advent of global positioning system (GPS) technology. It is now easy to obtain digital latitude and longitude readings from hand-held GPS devices. In 1978, the first global positioning satellites were launched by the *United States Air Force* to keep track of the geographical positions of ground vehicles, aircraft, and personnel. The average design-life of the satellites is 7.5 years, and a total of 40 have been built. At present, a constellation of 24 GPS-satellites orbit 1,200 miles above Earth. The satellites receive information on their ground

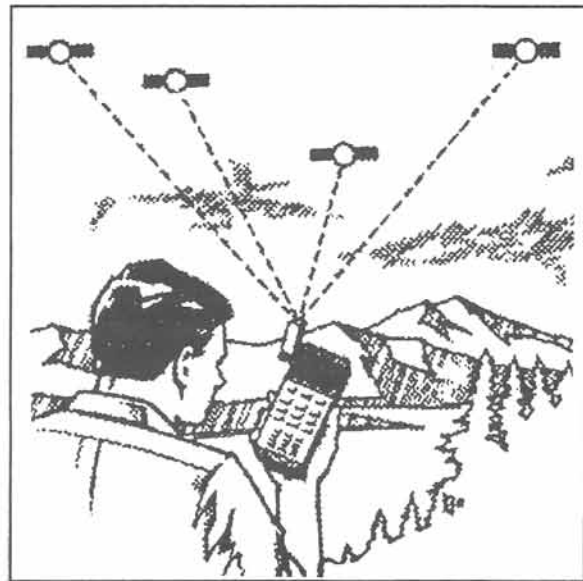


Figure 17-11: GPS satellite receiver uses signals from US Air Force satellites to triangulate ground positions.

positions from ground stations that control the system. The satellite positions are known and the distances to them are determined by highly accurate timing signals.

Each personal GPS-receiver takes data from at least three satellites to triangulate and calibrate the actual position of the receiver on the ground (Fig. 17-11). If four satellites are available, the altitude of a position can be obtained, as well. A ground position is specified in terms of the global geographic grid coordinates. The GPS-signals for civilian receivers commonly give accuracies within 100 meters between the actual coordinates and those received from GPS. For the military, which use a set of signals separate from civilian users, positions can be determined with much greater accuracy. Every time the GPS device is used in a new area, the apparatus position needs to be calibrated with respect to the orbiting satellites. This is achieved by entering the approximate coordinates for a ground position at a known location.

All data recorded with GPS coordinates can be downloaded into a GIS database using the geo-

graphical coordinates to locate data properly on the map. Distortions inherent in properly locating most field mapping data are reduced. Computerized image processing is now, also, possible in the field, using portable computers. Although these units add both weight and vulnerability to any outdoor trip in rough terrain, they reduce the data processing time back in the office. However, it is unwise to abandon the manual interpretation of geological maps altogether. Keep practicing manual methods, so that you can operate without digital support if such situations arise.

Geological data of conventional (non-digital) maps are best entered by optical scanning, adjusting for scale and distortions related to map projection. However, it is both costly and time-consuming to convert existing geological maps into digital format, if separation of various data sets in different data planes is required. This is due to the large volume of complex data commonly contained in professional geological maps. Ultimately, the precision of any final map accuracy is dependent on the spatial resolution of the input data, the scale of the final map, the way in

which incomplete geological boundaries have been interpreted, and the resolution of the printing hardware used to produce the hardcopy map. GIS software has tools to manipulate raster data and vector data, but the complexity of coding schemes obviously requires specialist knowledge to achieve good results.

17-5 Dynamic digital maps

The concept of the dynamic digital map utilizes the new possibilities offered by modern computer hardware by incorporating customized, pull-down menus, that allow interactive display of selected data. Dynamic digital maps contain a series of windows, each containing some component of the map. The windows include index maps, field images, zoom facilities, and scrolling options. The power of this approach can best be appreciated by studying the dynamic map of the Springerville Volcanic Field, Arizona, prepared by *Christopher Condit* and available on CD-ROM from the *Geological Society of America*. Pop-up windows display information on lithological units and locate specific samples within the map segment studied (Fig. 17-12).

All palettes can be moved to see the map beneath them. The software is based on Super-card, a hypermedia programming language. This environment has been used to write a presentation manager, a program designed to reformat digital maps into a package that maximizes user accessibility.

Dynamic digital maps may be based on GIS systems, but they, also, include multimedia accessories. For example, the dynamic map of Springerville includes photograph windows with

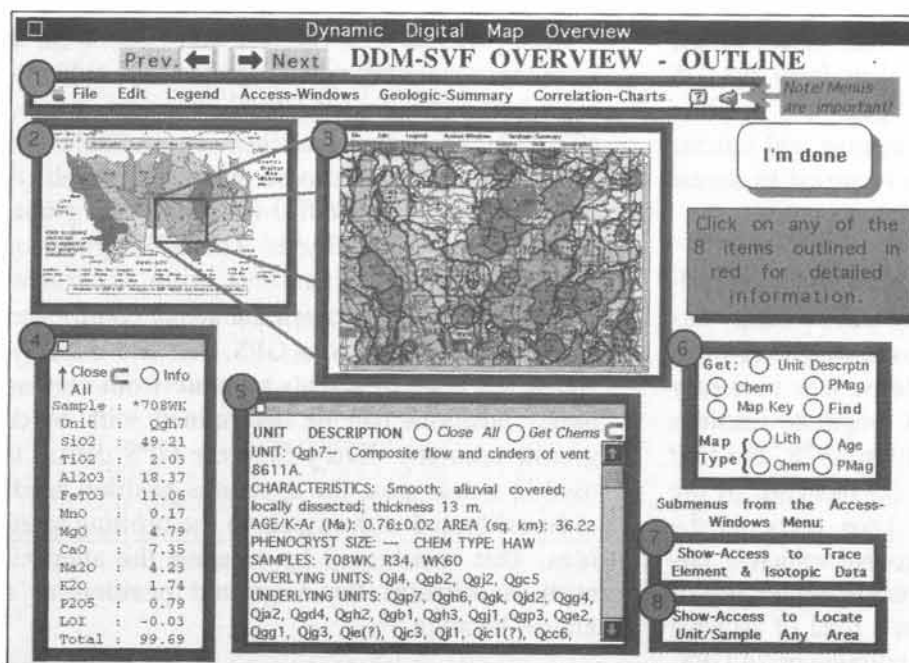


Figure 17-12: Major windows displayed in dynamic digital map of the Springerville Volcanic Field, Arizona.

oblique aerial views and outcrop close-ups. Other windows display introductory text. The hypermedia-aspect allows interactive linking of data within various parts of the map. For example, when the unit Qgh7 is highlighted, its spatial distribution, description, locations of rock samples, and chemical analysis can be quickly assessed. The dynamic geological map is programmed to provide menus that enable the user to have quick access to a variety of data. These data may include tables, videofilm, spoken text, and other attributes now available for multimedia presentations. Consequently, dynamic geoscience maps include a far broader range of material than the traditional hard-copy maps. The formatted CD-ROM is inexpensive to reproduce, with nominal cost between one and two US dollars for multiple copies. Digital maps can employ high-quality colors without the cost concern that sometimes impedes the production of hardcopy maps in color. Dynamic maps can be rapidly distributed electronically, using Internet facilities or local library networks, and enhance scientific productivity by reducing search time.

17-6 On-line resources for maps

Ordering CD-ROM, magnetic tapes, and other physical storage formats of digital map files is one way to acquire digital map data. But you can, also, try to surf cyberspace to access digital map files from a variety of sources. One of the primary functions of the Internet is file transfer. One way to transfer files is through server programs, such as Gopher, WAIS, or the World Wide Web, which provide interfaces to Internet's multiple resources. These servers are used to send and retrieve information across the Net. Others methods include e-mail, telnet, and other gateways. The simplest form of file transfer is through FTP (file transfer protocol).

In order to get the files, some versatility in cyberspace surfing is essential. Once you start, you may like it, and, after the initial novelty wears off, you may use it even for professional purposes. An excellent on-line document by *Bill Thoen* on resources for Earth Scientists via

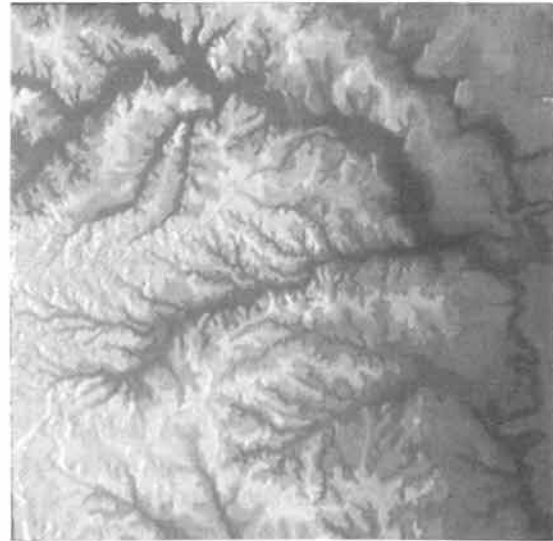


Figure 17-13: Landscape simulation, using USGS digital elevation data.

Internet is available (when this book went to press) via FTP from URL: <ftp://ftp.csn.org/COGS/ores.txt>. This list has been superceded by an HTML version on *Bill Thoen's* and *Ted Smith's* Web site at URL: <http://www.sni.net/~bthoen>. URL (universal resource locator) is a convention to represent each file address in a standard way. More information on URL's can be found in an article by *Tim Berner-Lee* at URL: <http://www.w3.org/pub/WWW/Addressing/URL/Overview.html> or by searching for *Berner-Lee*, using Gopher.

The *United States Geological Survey* has extensive on-line databases (Fig. 17-13). For example, ARC/INFO™ export files of US counties, derived from Census TIGER-files, can be accessed on-line (see information in URL: <ftp://ftp.csn.org/COGS/ores.txt>). The data in these files are derived from USGS 1:100,000 digital line graphs (DLG), complemented with older DIME data in metro areas. ARC/INFO™ itself is a GIS generating program written by the *Environmental Systems Research Institute*. More information is found at: URL: <http://www.esri.com/>

Information on Geographic Information Systems is available at URL: <http://ogis.org>. This

Web site is maintained by the *Open GIS Consortium*, which overall aim is to formulate compatible data formats for applications of GIS, Earth imaging, and other geo-processing technologies. *GISnet BBS* is an electronic bulletin board system that provides on-line resources for everyone interested in GIS, digital cartography, remote sensing, desktop mapping, and other earth science fields. Information on map data sets and other shareware is available at URL: <http://www.gisnet.com/gis/mapinfo/index.html>. On-line information on over 25,000 images of Earth from space and over 100 radar images from the Mission to Planet Earth can be found at URL: <http://www.csn.net/malls/rmdp>. Remote sensing imagery is, also, found at: URL: <http://www.coresw.com/>. Declassified CIA maps of the world are found at URL: <ftp://GIS.queensu.ca/pub/gis/cia/>. Other public domain maps, including DLG, DEM, DTM, and

TIGER files are at URL: <ftp://spectrum.xerox.com/pub/map/>. Although addresses may have changed by the time this book reaches you, be assured there is plenty of browsing material out there.

17-7 Interfacing platforms

Geoscientists in many industries, government agencies, and academia have experienced problems in getting data to and from their existing applications. The need for integration of databases is particularly pressing in the petroleum industry. For example, in order to monitor exploration developments, well-log data, residing in Geoshare files of *Schlumberger*, may need to be integrated with GIS maps of seismic lines, stored in ARC/INFO™. If additional information on production data is required, files with statistics on local and global industry data may need to be accessed. The simultaneous display of all these data can be achieved only through an interfacing platform. Such platforms aim to create a consistent environment for accessing and managing geoscience data.

Obviously, visualization technology plays a key role in developing integrated models of subsurface data. Visualizations of sophisticated reservoir models are used to enhance understanding and improve communication among the various specialists involved in reservoir analysis (Fig. 17-14). Comprehensive reservoir models must account for 3-D seismic and well-log stratigraphy, petrophysical properties, pore geometries, borehole images, permeability, saturation with natural and injected fluids, gravity, magnetics, radar, and other electromagnetic imagery. The models can include the kinematics of the system by showing temporal and spatial hydrocarbon migration paths (4-D models). The uncertainty of all these models varies and decreases with the spacing of the input data. Geostatistics can play an important role in the modeling effort by extrapolating various characteristics through reservoir volumes, away from well control points. Finally, all data must be integrated in one common format. This integration process makes building reservoir models can be very time-consum-

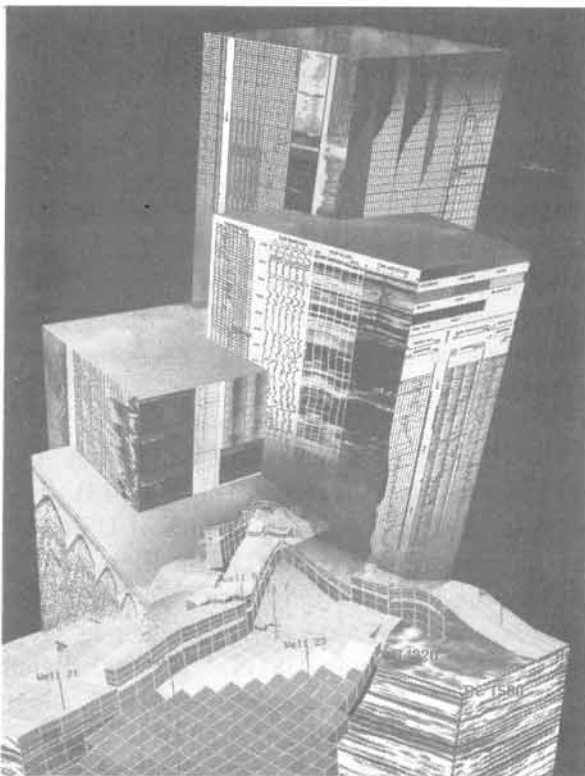


Figure 17-14: Artistic visualization of reservoir conditions by data integration on advanced imaging systems. Data visualization supports communication between geological experts.